CHAPTER V

RESULTS AND DISCUSSION

5.1 Degummed silk fiber

Silk consists of two main parts called silk sericin (silk gum) and silk fibroin. Silk sericin layer acts as an adhesive for the twin silk fibroin filaments and covers the luster of silk fibroin [6]. Many studies illustrated that the sericin glue-like proteins are the major cause of adverse problems with biocompatibility and hypersensitivity to silk [15]. Therefore, silk sericin must be removed to achieve pure silk fibroin fiber. Figure 5.1 showed SEM micrographs of silk fiber before and after degumming. Before degumming, the surface of cocoon fiber was rough (Figure 5.1(a)-(b)) which was the result of coated sericin layer. After sericin layer was removed by Na_2CO_3 [1], the surface of fiber was smooth as shown in Figure 5.1(c)-(d). Figure 5.1(e)-(f) showed the degummed silk fiber with NaOH [60]. The fiber surface was not smooth implying either an incomplete removal of sericin or damaged fibers by NaOH. From this qualitative result, degummed silk fiber using Na_2CO_3 was chosen for further uses.

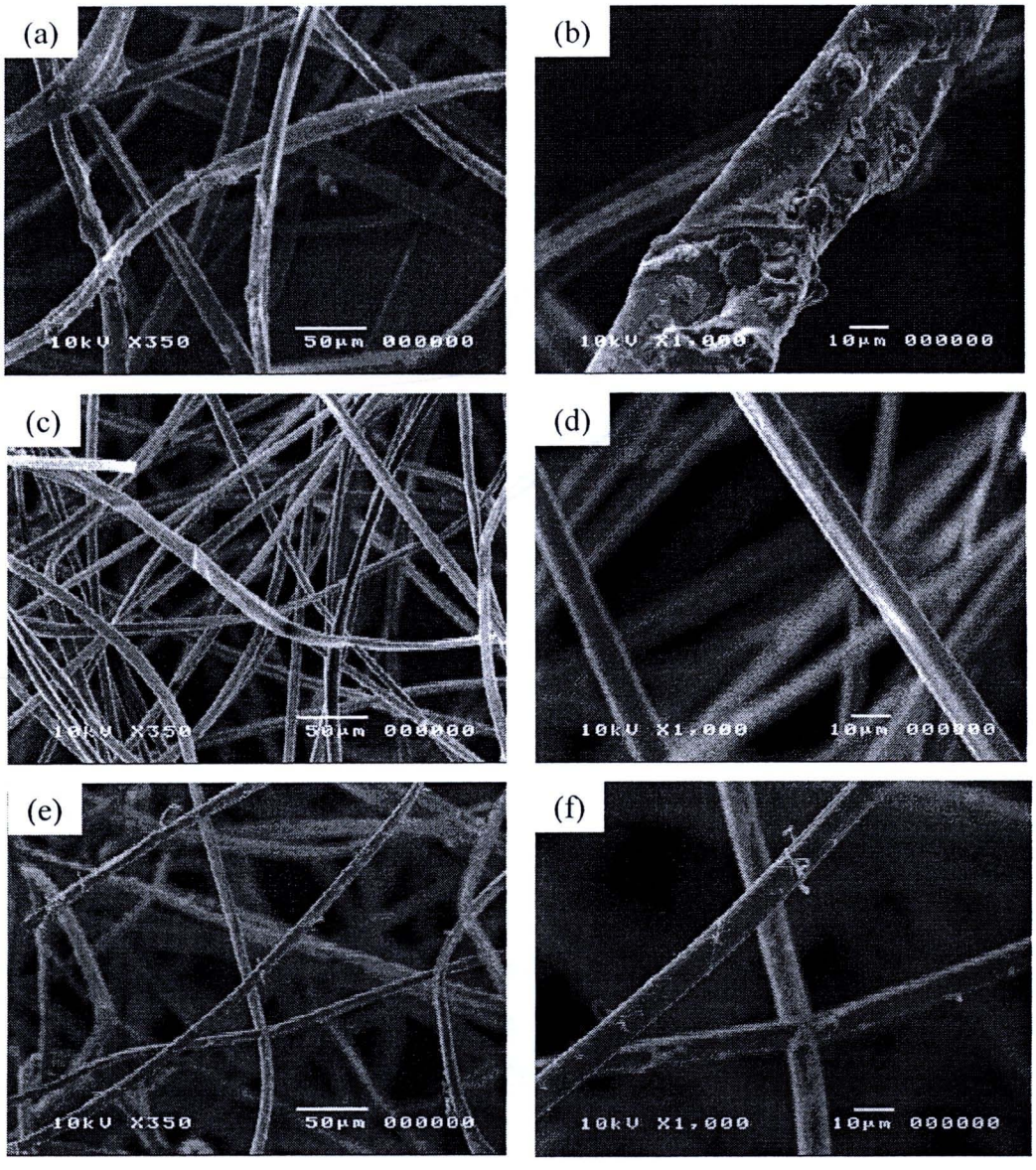

Figure 5.1 SEM micrographs of silk fiber: (a)-(b) cocoon fiber, (c)-(d) degummed silk fiber with Na_2CO_3, and (e)-(f) degummed silk fiber with NaOH.

5.2 Chemical characteristics of silk fibroin scaffolds

After dialysis process, silk fibroin solution was fabricated into scaffolds by freeze-drying and salt-leaching methods. Chemical characteristics of silk fibroin scaffolds were examined by attenuated total reflection fourier transform infrared (ATR-FTIR) spectrophotometric and X-ray diffraction (XRD) techniques. In addition, LiBr residual in silk fibroin scaffolds was investigated by XRD.

5.2.1 Structural analysis of silk fibroin scaffolds

5.2.1.1 Attenuated total reflection fourier transform infrared (ATR-FTIR) spectrophotometric analysis

ATR-FTIR spectra of freeze-dried silk fibroin scaffolds were shown in Figure 5.2(a)-(c). It could be seen that the peak positions of amide I (C=O stretching), amide II (N–H deformation and C–N stretching), and amide III (C–N stretching and N–H deformation) were located at 1645, 1530, and 1238 cm^{-1}, respectively. These amide bands attributed to the primary structure (random coil) of silk fibroin [41]. This could be reflected from silk fibroin molecules in aqueous solution [44]. In other words, dehydrothermal (DHT) and chemical (EDC) treatments of silk fibroin scaffolds did not induce the transition of secondary structure of silk fibroin. Yamada *et.al.* [61] reported that the structural change of regenerated silk fibroin on heating occurred at approximately 200°C. Therefore, DHT treatment at 140°C was ineffective to structural transition of silk fibroin scaffolds. Generally, EDC was known as a crosslinking agent for proteins. EDC activates the carboxyl group of glutamic or aspartic acid to form an active O-acylisourea intermediate which reacts with an amino group [63]. Sofia *et.al.* [47] stated that EDC treatment led to more stable amide formation of silk fibroin. However, in our ATR-FTIR result, no change in structure of silk fibroin scaffolds due to EDC treatment was detected. Figure 5.2(d) showed ATR-FTIR spectrum of air-dried silk fibroin after gelling. The

absorption bands of amide I approximately at 1625 cm^{-1}, amide II at 1520 cm^{-1}, and amide III at 1265 cm^{-1} were observed. The peak positions of these amide bands reflected the secondary structure (β-sheet) of silk fibroin [55, 64]. This is consistent to several works demonstrated that the structure of silk fibroin was transformed from random coil to β-sheet after gelation process [1, 40, 49, 51]. Gelation process was believed to cause the shift of peak position of amide bands within silk fibroin molecules. ATR-FTIR results revealed that different fabrication process resulted in a difference in the secondary structure of silk fibroin scaffolds.

5.2.1.2 X-ray diffraction (XRD) analysis

Figure 5.3 showed X-ray diffraction patterns of freeze-dried silk fibroin and air-dried silk fibroin scaffolds after gelling. When silk fibroin aqueous solutions were freeze-dried, no peak was detected (Figure 5.3(a)) implying that freeze-dried silk fibroin scaffolds exhibited an amorphous structure [49]. Meanwhile silk fibroin scaffolds after DHT treatment displayed the same pattern as before the treatment as seen in Figure 5.3(b). This corresponded to ATR-FTIR results, e.g. freeze-drying and DHT treatment did not significantly influence the structure of silk fibroin. After treatment with EDC, the XRD peak appeared at $2\theta=20^{o}$ as presented in Figure 5.3(c). This might be the effect of the primary amines on the peptides formed a stable amide bond between the peptide of gelatin and silk fibroin [47]. Air-dried silk fibroin scaffolds after gelling showed a sharp peak at $2\theta=20.6^{o}$ and a small peak at $2\theta=24^{o}$. These peaks represented the β-sheet structure of silk fibroin [1, 40, 49, 51, 55]. The other peak at $2\theta=9^{o}$ that indicated β-sheet was not observed in our result due to the limitation of the equipment.

From the results of X-ray diffraction, the gelation of silk fibroin solutions induced a transition from random coil to β-sheet structure. This result corresponded to the ATR-FTIR spectra of silk fibroin scaffolds as discussed in section 5.2.1.1. The results on ATR-FTIR and XRD rendered that the structure of freeze-dried silk fibroin scaffolds was random coil while that of air-dried silk fibroin scaffolds after gelling was β-sheet.

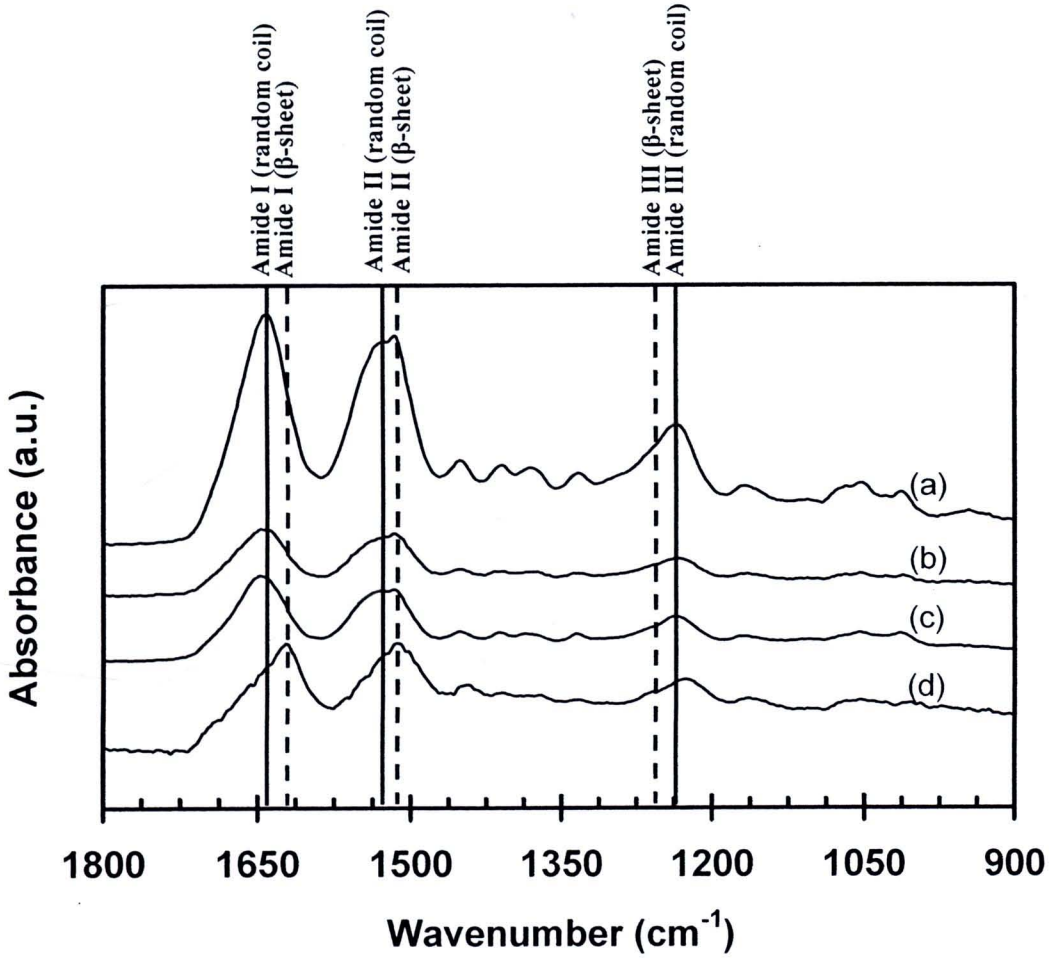

Figure 5.2 ATR-FTIR spectra of freeze-dried silk fibroin scaffolds from dialyzed solution (a) after freeze-drying (before any treatments), (b) after DHT treatment for 48 h, (c) after DHT and EDC treatments, and (d) air-dried silk fibroin obtained after gelling.

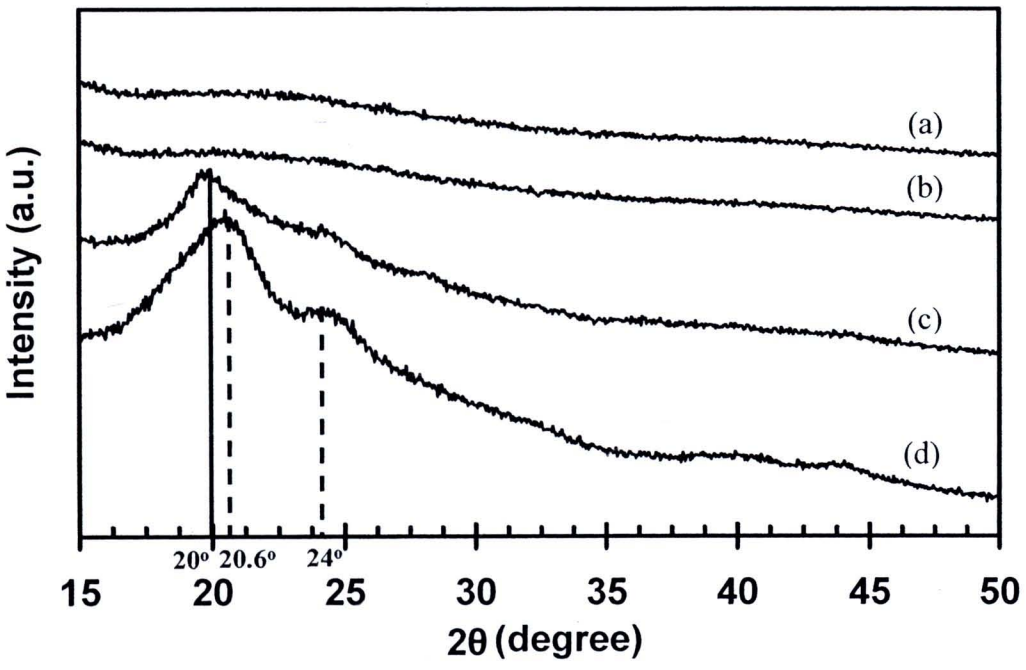

Figure 5.3 XRD patterns of freeze-dried silk fibroin scaffolds from dialyzed solution (a) after freeze-drying (before any treatments), (b) after DHT treatment for 48 h, (c) after DHT and EDC treatments, and (d) air-dried silk fibroin obtained after gelling.

5.2.2 LiBr residual in silk fibroin scaffolds

Figure 5.4 showed X-ray diffraction pattern of lithium bromide (LiBr) powder. The peak position appeared at 2θ=27, 32, and 46°. These positions could not be observed in the XRD patterns of silk fibroin scaffolds (Figure 5.3). This confirmed that there was no LiBr residual in silk fibroin scaffolds.

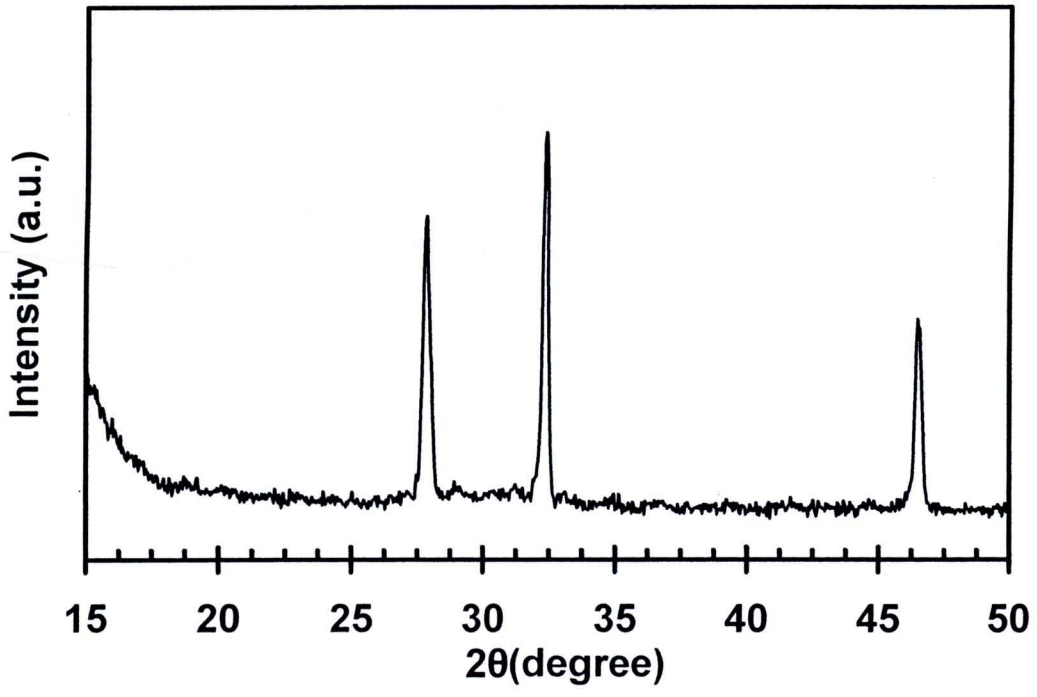

Figure 5.4 XRD pattern of lithium bromide (LiBr) powder.

5.3 Comparison of type A and type B gelatin blending in silk fibroin

After silk fibroin aqueous solution was obtained from dialysis process, the blending of silk fibroin solution with each type of gelatin was investigated and the resulting scaffolds were compared. Either type A or type B gelatin was blended with silk fibroin solution at various blending weight ratios and gelatin/silk fibroin scaffolds were

obtained by freeze-drying. After DHT and EDC treatments, silk fibroin and gelatin/silk fibroin scaffolds were cross-sectional cut in order to observe the morphology under SEM. Figure 5.5 demonstrated SEM micrographs of type B gelatin/silk fibroin scaffold. It could be seen that pure silk fibroin scaffolds possessed highly interconnected porous network, as presented in Figure 5.5(a)-(b), while pure gelatin scaffolds, presented in Figure 5.5(o)-(p), showed leave-like porous structure with very low interconnection.

When silk fibroin was blended with type B gelatin as shown in Figure 5.5(c)-(n), non-uniform porous structure of scaffolds was observed. Two layers were distinguished in cross-sectional scaffolds; the upper layer consisted of a lot of small fibrous pores around big leave-like pores while the lower layer was mainly leave-like porous structure. This implied an incompatibility of silk fibroin and type B gelatin.

Figure 5.6 depicted SEM micrographs of type A gelatin/silk fibroin scaffolds. It could be noticed that the porous structure of type A gelatin/silk fibroin scaffolds at each blending ratio was uniform. The interconnected porous network of type A gelatin/silk fibroin scaffolds was less than that of pure silk fibroin scaffolds. A more amount of gelatin in the scaffolds resulted in less fibrous network, less interconnection, and bigger pores similar to the leave-like porous structure of type A gelatin (pore size ~50-150μm).

The morphology of gelatin/silk fibroin scaffolds revealed in Figure 5.5 and 5.6 proved that only type A gelatin could be homogeneously blended with silk fibroin. This was a result from the charges of materials which depended upon pH and pI, as illustrated in Table 5.1.

Table 5.1 pI and charges of silk fibroin and gelatin

Materials	pI	Charge at pH ~5.5-6
Silk fibroin	~3	Anionic
Type A gelatin	~9	Cationic
Type B gelatin	~5	Anionic

At the working pH ~5.5-6, silk fibroin and type B gelatin have anionic charges while type A gelatin employs cationic charge. An electrostatic interaction between silk

fibroin and type A gelatin is therefore formed, resulting in a homogeneous blended solution and scaffold structure. On the other hand, repulsive force between silk fibroin and type B gelatin is the main reason for non-uniform blended solution and scaffold structure. Therefore, type A gelatin was chosen to incorporate with silk fibroin in this work. For further investigation, the word "gelatin" was referred to "type A gelatin".

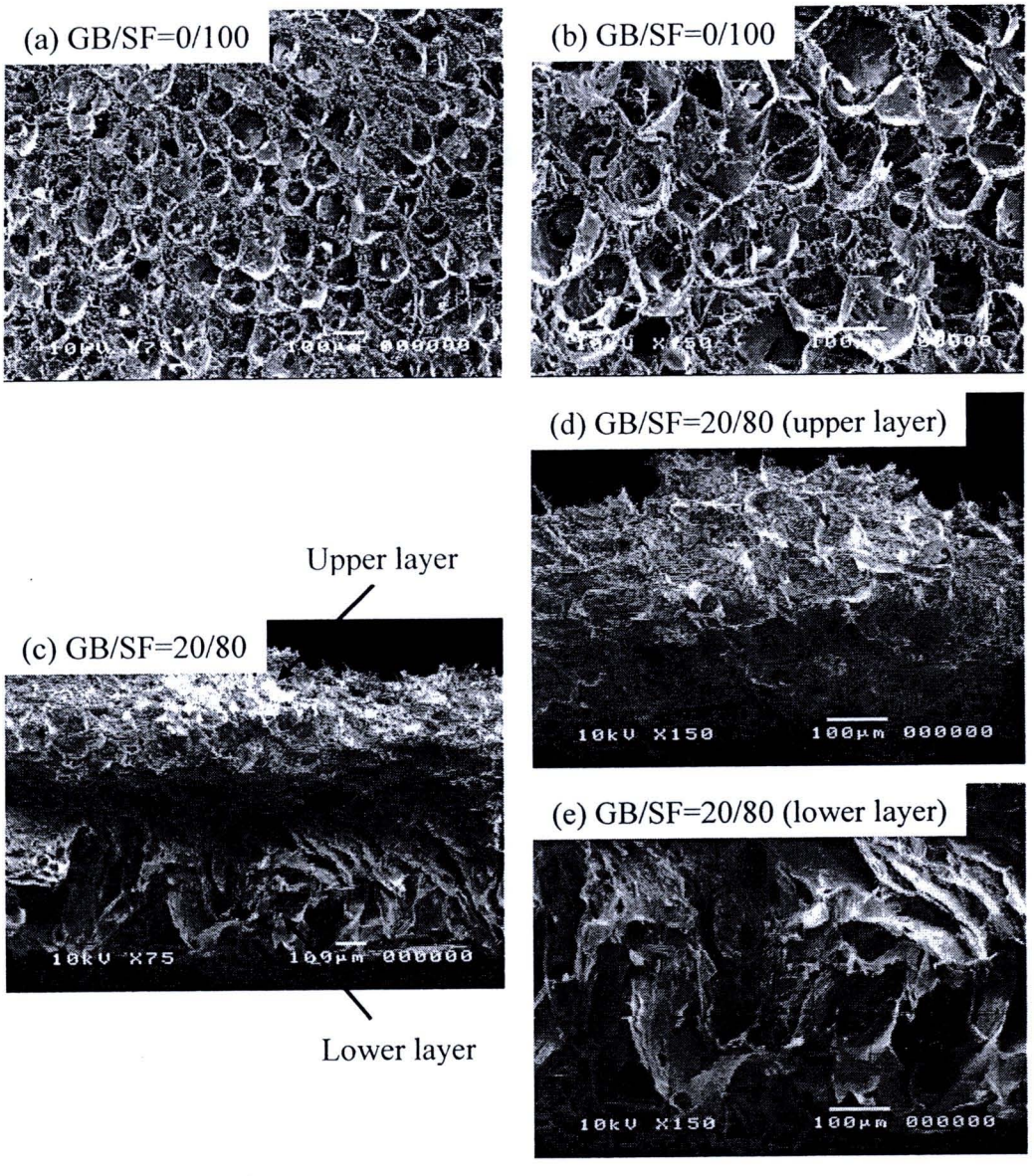

(g) GB/SF=40/60 (upper layer)

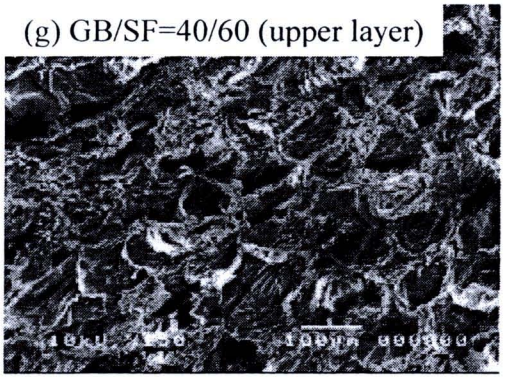

Upper layer

(f) GB/SF=40/60

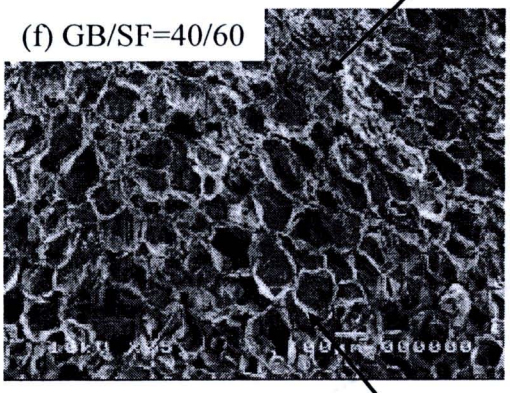

Lower layer

(h) GB/SF=40/60 (lower layer)

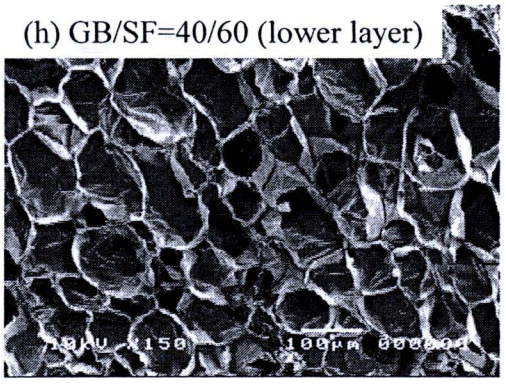

(j) GB/SF=60/40 (upper layer)

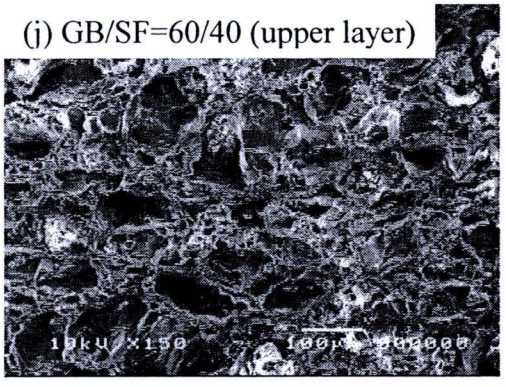

Upper layer

(i) GB/SF=60/40

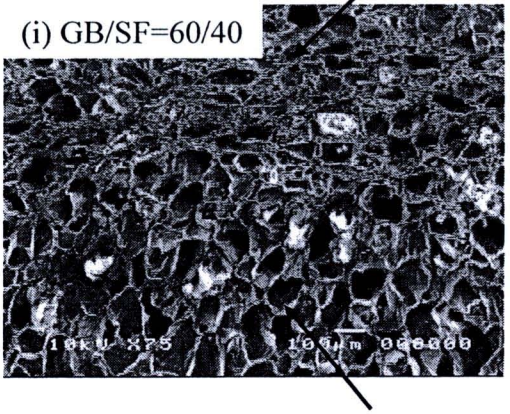

Lower layer

(k) GB/SF=60/40 (lower layer)

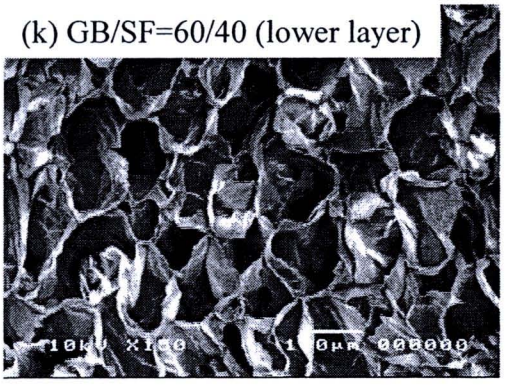

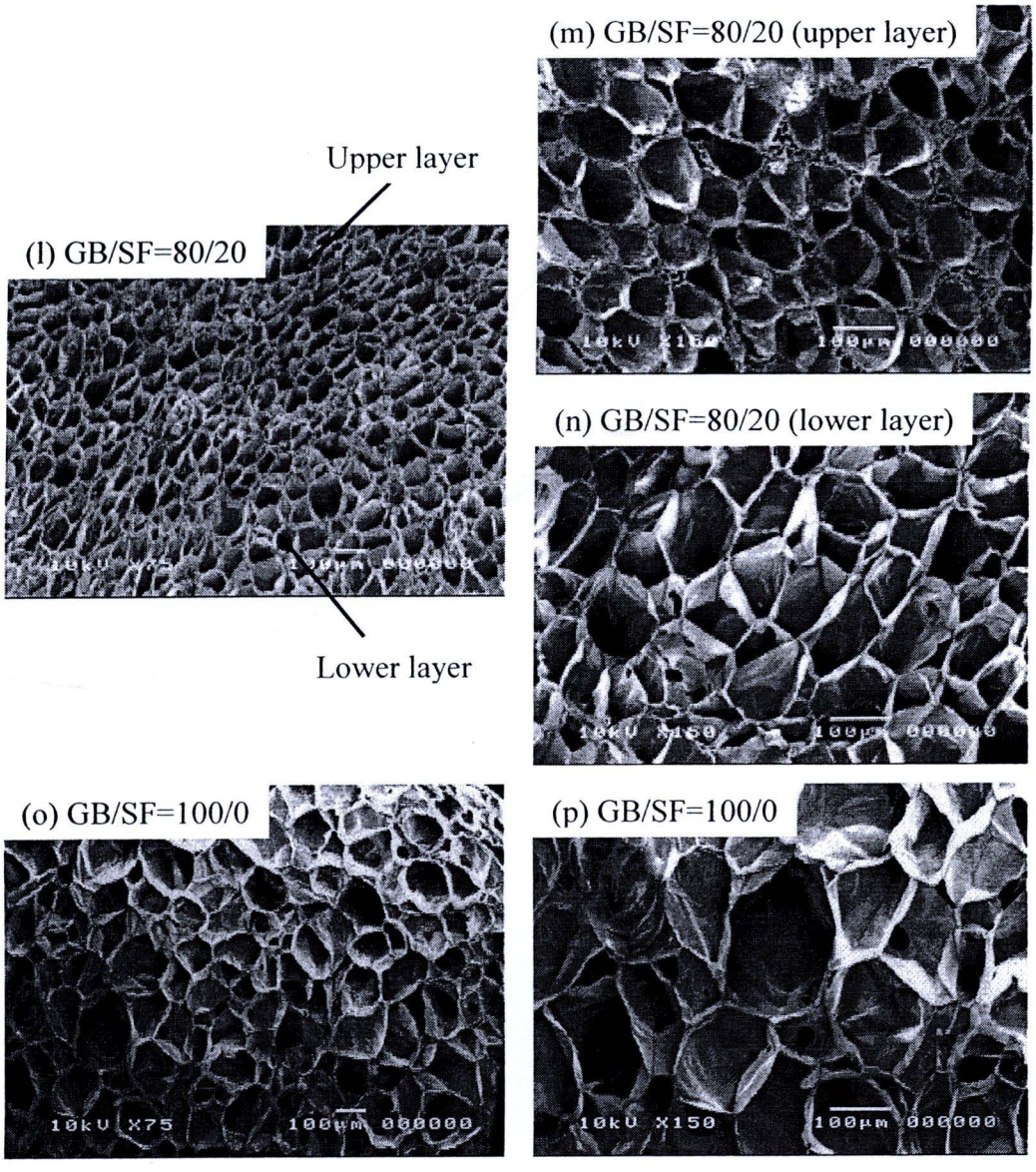

Figure 5.5 SEM micrographs of freeze-dried type B gelatin/silk fibroin (GB/SF) scaffolds (a), (b) 0/100, (c)-(e) 20/80, (f)-(h) 40/60, (i)-(k) 60/40, (l)-(n) 80/20, and (o), (p) 100/0.

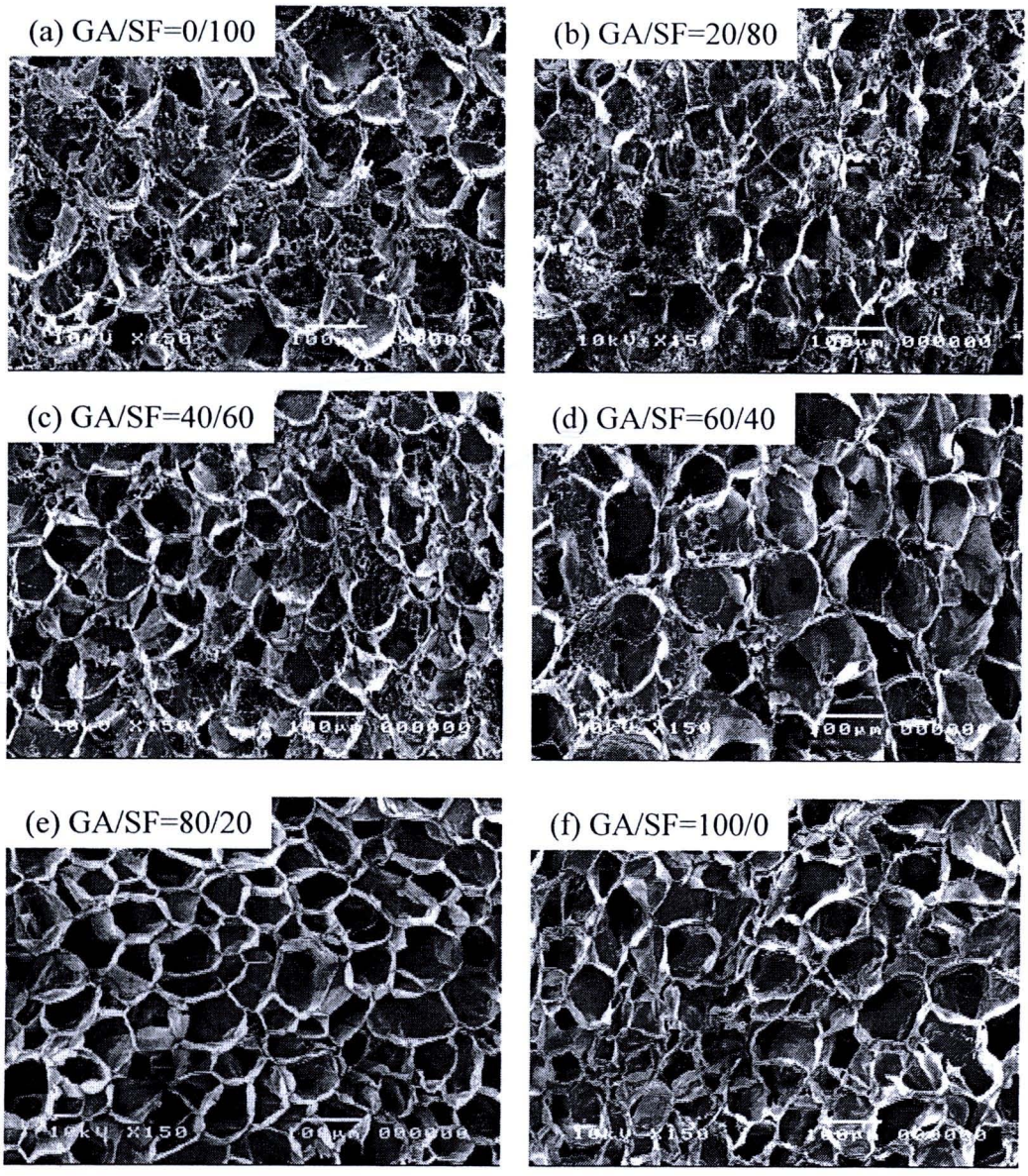

Figure 5.6 SEM micrographs of freeze-dried type A gelatin/silk fibroin (GA/SF) scaffolds (a) 0/100, (b) 20/80, (c) 40/60, (d) 60/40, (e) 80/20, and (f) 100/0.

5.4 Silk fibroin and gelatin/silk fibroin scaffolds via freeze-drying

As the morphology of type A gelatin/silk fibroin blended scaffolds at various blending weight ratios has been presented and discussed in section 5.3. In this section, other characterizations of these blends were presented and discussed. Furthermore, the effects of the dehydrothermal treatment periods at 140°C for 24 and 48 h prior to EDC treatment were investigated.

5.4.1 Compressive modulus of scaffolds

The compressive modulus of gelatin/silk fibroin scaffolds with various dehydrothermal treatment periods was illustrated in Figure 5.7. When the scaffolds were DHT treated for 24 h prior to EDC treatment, the compressive modulus of freeze-dried pure silk fibroin and gelatin scaffolds were 442.50±66.52 and 302.50±34.03 kPa, respectively. It was found that the compressive modulus of pure silk fibroin scaffolds was higher than that of pure gelatin and all gelatin/silk fibroin scaffolds except gelatin/silk fibroin scaffold at blending ratio 20/80 which possessed the highest compressive modulus among all freeze-dried scaffolds. There was a significant difference in the compressive modulus of scaffolds at all blending ratio relative to pure gelatin scaffolds. When the scaffolds were DHT treated for a longer period of 48 h prior to EDC treatment, the compressive modulus of freeze-dried pure silk fibroin and gelatin scaffolds were 350.00±102.31 and 337.14±143.96 kPa, respectively. These are about the same as those scaffolds DHT treated for 24 h. Additionally, the compressive modulus of all blended scaffolds were similar to those processed in DHT treatment for 24 h. In other words, there was no significant difference in the compressive modulus of each type of scaffolds when DHT treated for 24 and 48 h.

Generally, the mechanical characteristic of scaffolds depended upon the type of materials and the structure of scaffolds. The results indicated that the blending ratio

affected the compressive modulus of the scaffolds. Scaffolds with high silk fibroin content (80-100%) possessed relatively high compressive modulus.

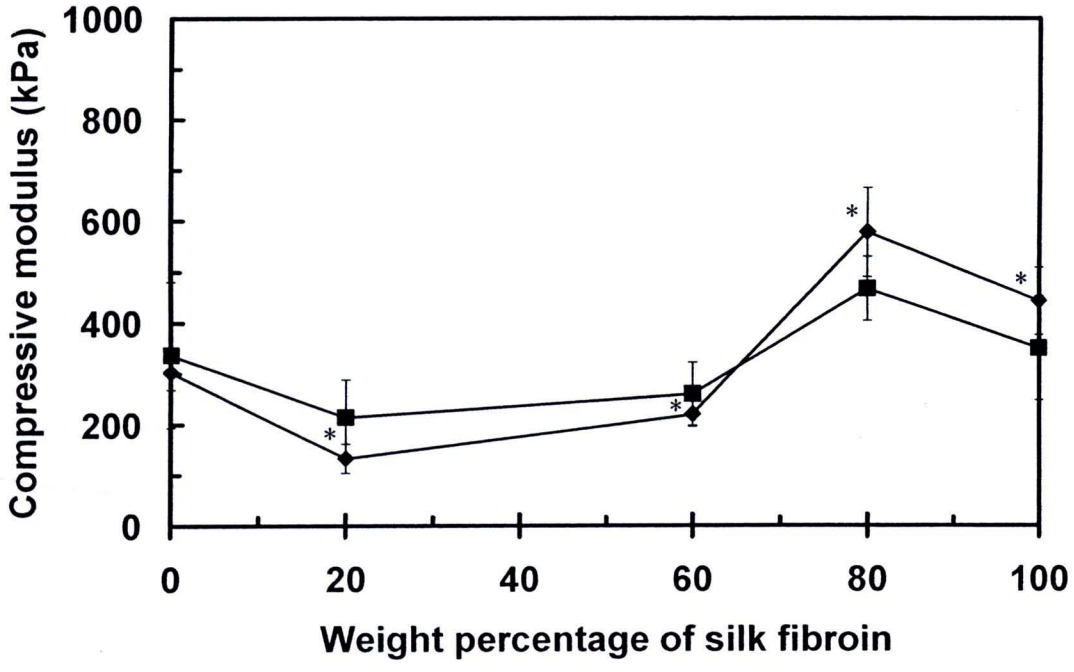

Figure 5.7 Compressive modulus of freeze-dried gelatin/silk fibroin scaffolds with various DHT treatment periods: (♦) 24 h, and (■) 48 h.

* represent the significant difference ($p<0.05$) relative to gelatin scaffolds.

§ represent the significant difference ($p<0.05$) relative to the same weight percentage of silk fibroin.

5.4.2 Swelling property of scaffolds

The swelling ratios of the scaffolds represented the amount of water uptake to the dry weight of scaffolds. Swelling ability was an important property for tissue engineering to absorb cell and transport nutrient into scaffolds. Figure 5.8 showed swelling ratios of gelatin/silk fibroin scaffolds with various DHT treatment periods. While 24 h of DHT treatment was employed, it could be seen that swelling ratios of freeze-dried pure silk

fibroin and gelatin scaffolds were 9.19±1.34 and 12.01±0.60, respectively. The result on the swelling ratio of gelatin scaffolds corresponded to the work of Ratanavaraporn [8]. She reported that the swelling ratios of 0.8wt% freeze-dried type A gelatin scaffolds was 16.64±6.09 and this ration decreased as decreasing gelatin concentration. The swelling ratio of pure silk fibroin scaffolds was significantly lower than that of pure gelatin scaffolds. This could due to the hydrophobic property of silk fibroin. As expected, swelling ratios of gelatin/silk fibroin scaffolds tended to slightly decrease as increasing silk fibroin content. Similarly, the swelling ratios of scaffolds DHT treated for 48 h were closed to those with 24 h of DHT treatment. This result demonstrated that DHT treatment period had no effects on the swelling property of scaffolds.

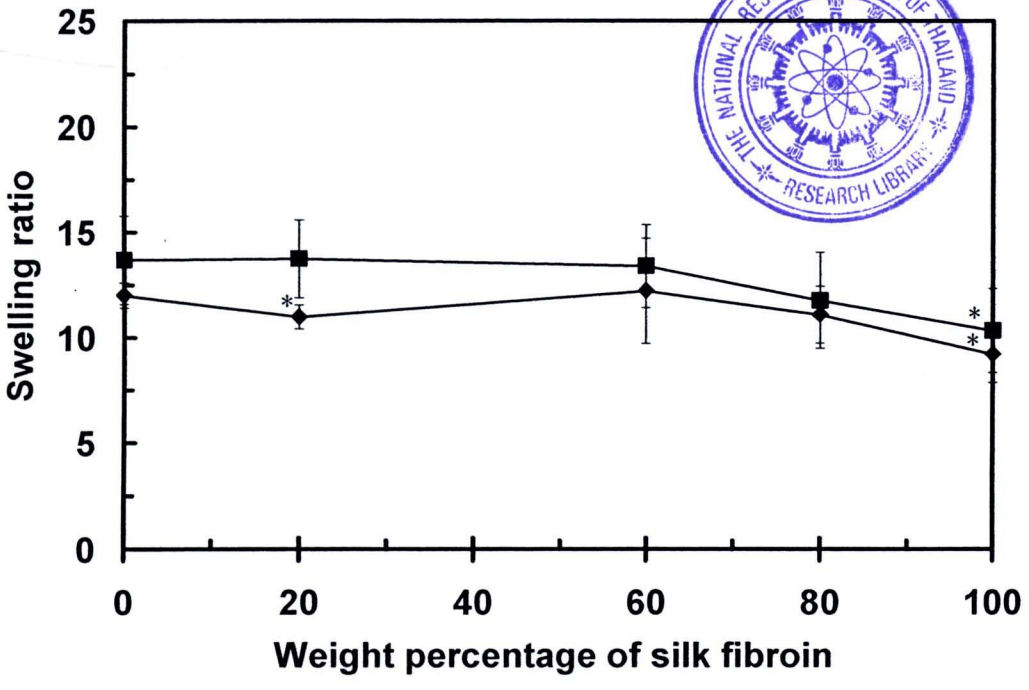

Figure 5.8 Swelling ratios of freeze-dried gelatin/silk fibroin scaffolds with various DHT treatment periods: (♦) 24 h, and (■) 48 h.

* represent the significant difference ($p<0.05$) relative to gelatin scaffolds.

§ represent the significant difference ($p<0.05$) relative to the same weight percentage of silk fibroin.

5.4.3 Biological property of scaffolds

To evaluate biocompatibility of scaffolds, each scaffold was seeded with MSCs and MC3T3-E1 at a density of 2×10^4 cells per scaffold. Cell proliferation on scaffolds was investigated using MTT assay.

5.4.3.1 MSCs proliferation tests

The results on *in vitro* cell proliferation of MSCs on gelatin/silk fibroin scaffolds were shown in Figure 5.9. Due to a limit in the number of MSCs, the viability of cells on all scaffolds was determined only after 3 and 7 days of the culture. At 3 days after seeding, the number of cells on pure silk fibroin scaffold was less than pure gelatin and all blended scaffolds. There was no significant difference in the number of cells among various types of scaffolds. After 7 days of seeding, there were more MSCs on each type of scaffolds comparing to those at 3 days of culture. The highest increase in the number of MSCs from the 3rd to 7th date after seeding was obviously noticed for pure silk fibroin scaffolds. There was still no significant difference in the number of cells on all scaffolds after 7 days of culture. However, pure silk fibroin tended to have a slightly more proliferated MSCs comparing to gelatin/silk fibroin and gelatin scaffolds even it was not statistically different. This could due to the morphology of scaffolds (Figure 5.6). Freeze-dried pure silk fibroin scaffolds were a porous network with highly interconnection. This might support cell proliferation.

5.4.3.2 MC3T3-E1 proliferation tests

Figure 5.10 showed the numbers of MC3T3-E1 on gelatin/silk fibroin scaffolds after 1, 7 and 14 days of the culture. At 1 day after seeding, the number of cells on pure silk fibroin scaffold was higher than that of pure gelatin and all gelatin/silk fibroin scaffolds except gelatin/silk fibroin scaffold at blending ratio 20/80. This could be a

result from the morphology of scaffolds (Figure 5.6). Scaffolds with high silk fibroin content (80-100%) had highly interconnected porous network. This might support cell migration. At 7 days after seeding, there was more MC3T3-E1 on each type of scaffolds comparing to those at 1 days of culture. The number of cell on pure silk fibroin and gelatin scaffolds increased 140%, and 2400%, respectively. However, there was no significant difference in the number of osteoblast-like cells on all types of scaffolds. This implied that, in this case, blending of gelatin that was known to contain RGD-like sequence could not promote cell proliferation. The pattern of the number of osteoblast cells grown on all scaffold after 7 days of seeding was similar to that noticed when using MSCs (Figure 5.9). At 14 days after MC3T3-E1 seeding, the same trend as that after 7 days of seeding was observed. Nevertheless, the number of cells tended to slightly decrease in blended scaffolds as increasing silk fibroin content.

This result demonstrated that both cell types can proliferate on freeze-dried gelatin/silk fibroin scaffolds with a similar number.

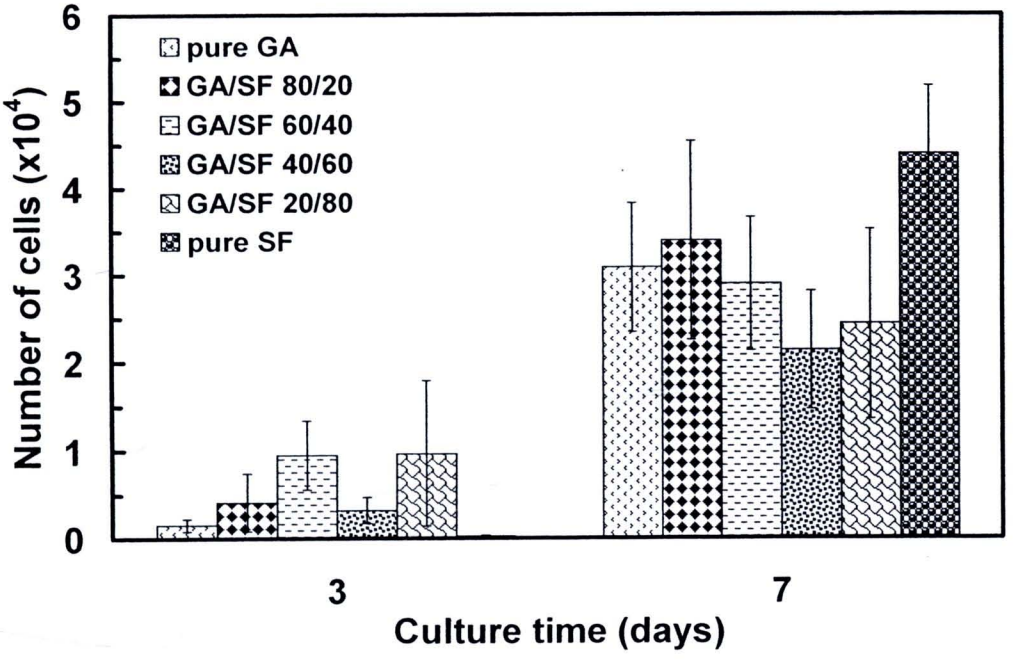

Figure 5.9 Number of MSCs on freeze-dried gelatin/silk fibroin scaffolds after 3 and 7 days of the culture (seeding: 2×10^4 cells/scaffold).

* represent the significant difference ($p<0.05$) relative to gelatin scaffolds in each periods.

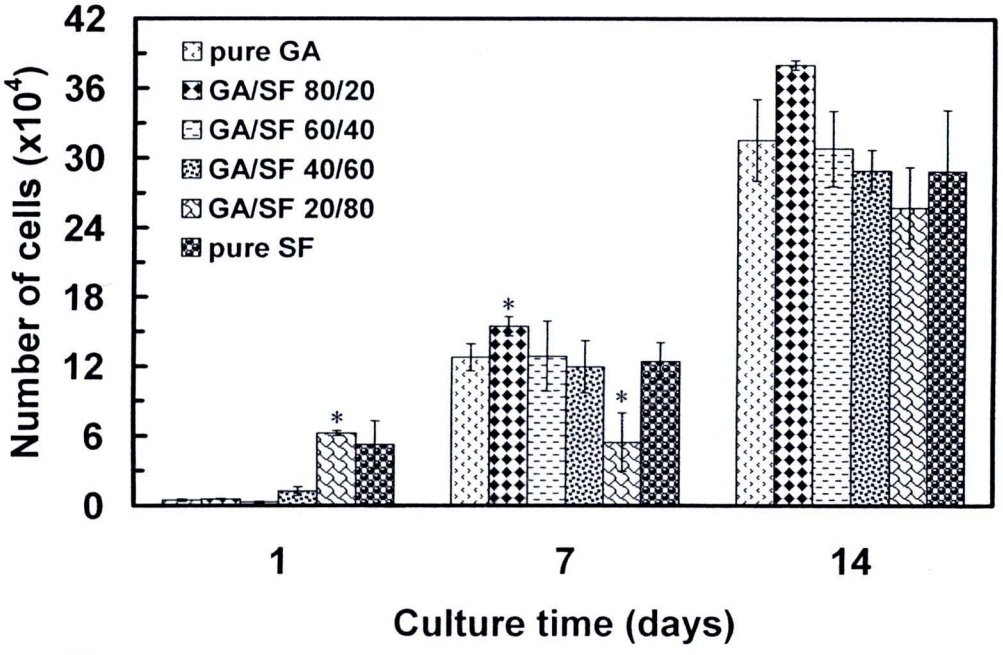

Figure 5.10 Number of MC3T3-E1 on freeze-dried gelatin/silk fibroin scaffolds after 1, 7, and 14 days of the culture (seeding: 2×10^4 cells/scaffold).
* represent the significant difference ($p<0.05$) relative to gelatin scaffolds in each periods.

5.4.3.3 MC3T3-E1 migration and morphological observation

The morphology of MC3T3-E1 cultured on 20/80 gelatin/silk fibroin and pure silk fibroin scaffolds for 14 days were depicted in Figure 5.11 and 5.12, respectively. These two were selected for cell-material morphological observation since they did not collapse after dehydration with ethanol and hexamethyldisilazane (HMDS). MC3T3-E1 migration was investigated from the cell seeding side (position 1-Figure 5.11(a) and Figure 5.12(a)) down to the plate-exposed side (position 4-Figure 5.11(d) and Figure 5.12(d)). The micrographs demonstrated that MC3T3-E1 could penetrate through the thickness of both scaffolds. Cells could be observed on the scaffold from cell seeding side toward bottom side. Using higher magnification, cell morphology on 20/80

gelatin/silk fibroin and pure silk fibroin scaffolds after 14 days of culture was shown in Figure 5.13. Interaction between the cells and the surfaces of scaffolds was noticed. MC3T3-E1 proliferated on the surface of 20/80 gelatin/silk fibroin scaffolds were round and a sign of filopedia was noticed in Figure 5.13(a). On the other hand, no filopodia evidence was observed on pure silk fibroin surface as shown in Figure 5.13(b). This phenomenon could demonstrate a difference in the ability of cells to proliferate on the surface of 20/80 gelatin/silk fibroin and pure silk fibroin scaffolds.

This result on in vitro cell culture of freeze-dried scaffolds illustrated that cell types, material, blending composition of material including morphology of scaffolds influenced cell proliferation.

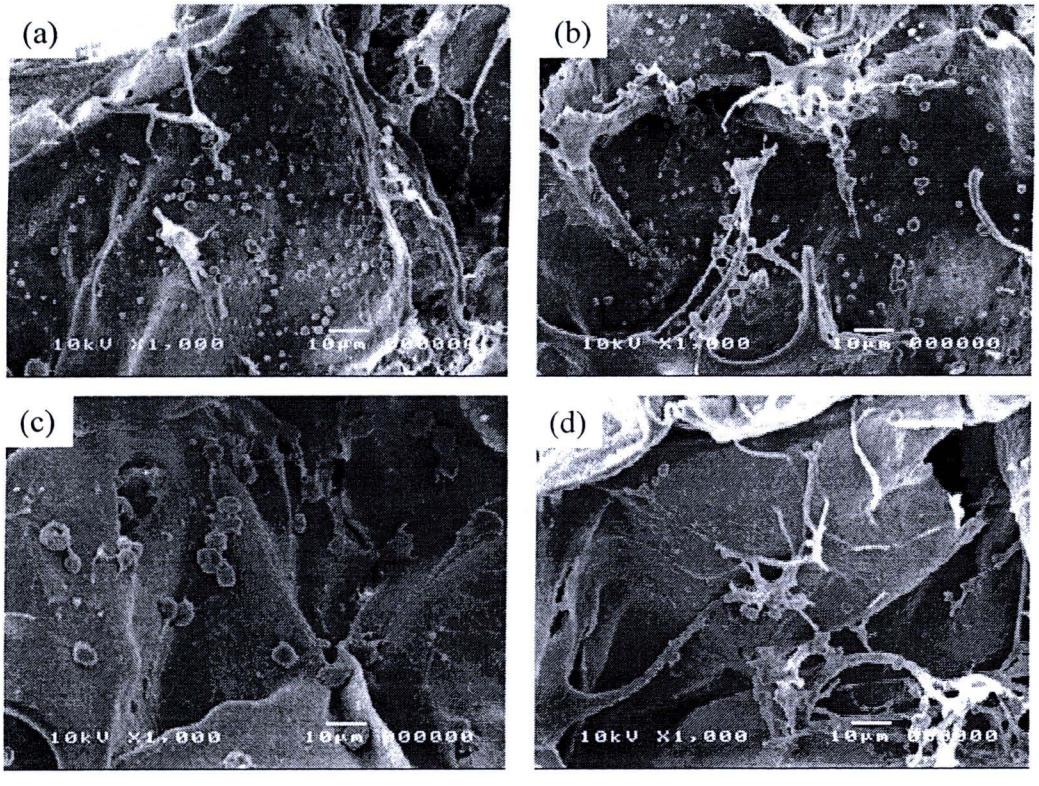

Figure 5.11 SEM micrographs of cross-sectional plane of freeze-dried 20/80 gelatin/silk fibroin scaffolds at position (a) 1 (cell seeding side), (b) 2, (c) 3, and (d) 4 (plate-exposed side) after 14 days of MC3T3-E1 culture.

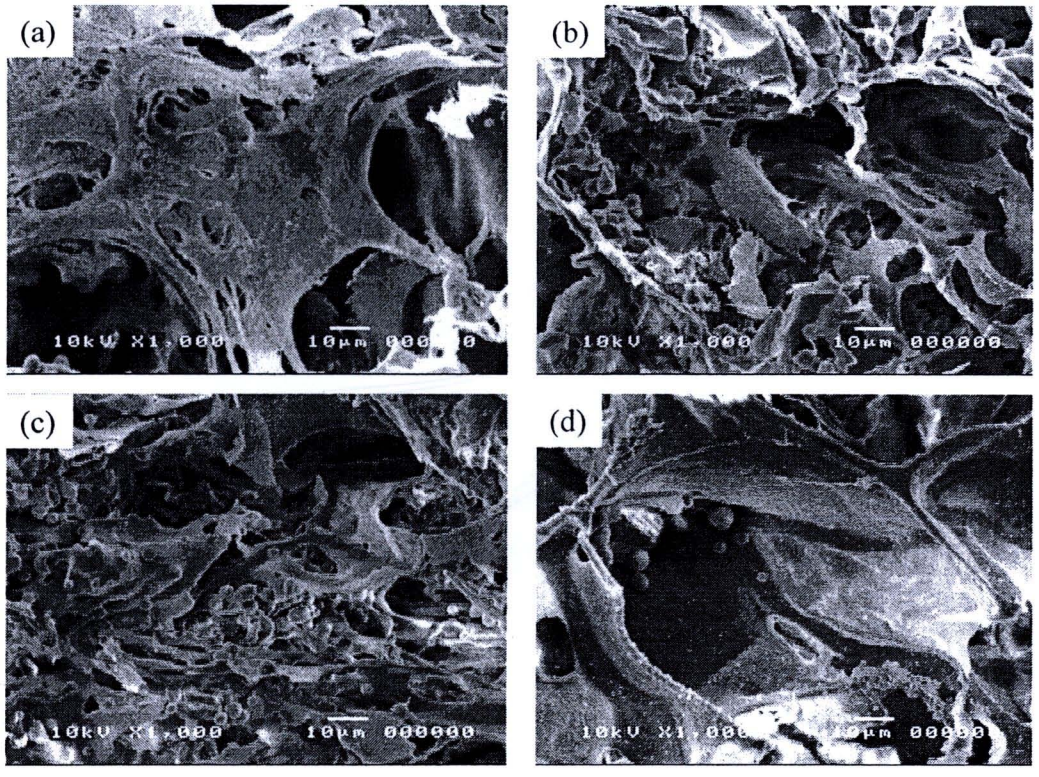

Figure 5.12 SEM micrographs of cross-sectional plane of freeze-dried pure silk fibroin scaffolds at position (a) 1 (cell seeding side), (b) 2, (c) 3, and (d) 4 (plate-exposed side) after 14 days of MC3T3-E1 culture.

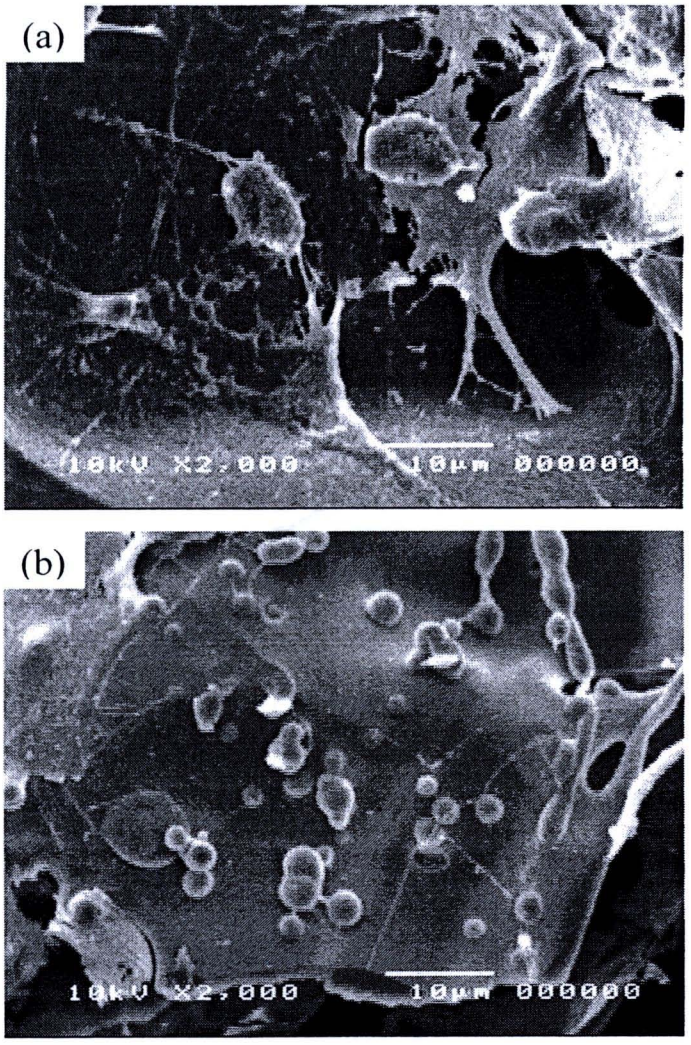

Figure 5.13 SEM micrographs of MC3T3-E1 morphology after 14 day cultured on freeze-dried gelatin/silk fibroin scaffolds: (a) 20/80, and (b) 0/100.

5.5 Silk fibroin and conjugated gelatin/silk fibroin scaffolds via salt-leaching

In this section, porous silk fibroin scaffolds were prepared using salt-leaching method. The pore size of scaffolds could be regulated by the size of granular NaCl added into the silk fibroin aqueous solution. In this work, the size of granular NaCl used was 600-710μm (Figure 5.14) due to local availability.

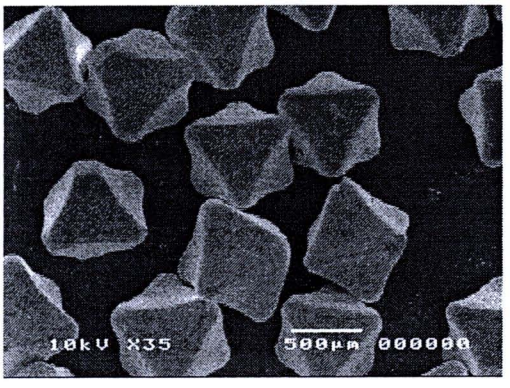

Figure 5.14 SEM micrograph of NaCl crystals.

After salt-leached silk fibroin scaffolds were obtained, surface was modified by conjugating with type A gelatin. Furthermore, silk fibroin and conjugated gelatin/silk fibroin scaffolds were alternately immersed in calcium and phosphate solution to allow the deposition of hydroxyapatite compound on the surface of scaffolds. This method was employed to grow hydroxyapatite compound on various surface of substrates [11, 56-57]. All types of salt-leached scaffolds prepared were listed in Table 5.2.

Table 5.2 Salt-leached scaffolds prepared in this work

Scaffolds	Number of alternate soaking cycles	Notation
Silk fibroin scaffolds	0	SF0
	2	SF2
	4	SF4
	6	SF6
Conjugated gelatin/silk fibroin scaffolds	0	CGSF0
	2	CGSF2
	4	CGSF4
	6	CGSF6

5.5.1 Morphology of scaffolds

5.5.1.1 Hydroxyapatite/silk fibroin scaffolds

Figure 5.15 showed the cross sectional morphology of hydroxyapatite/silk fibroin scaffolds. Before hydroxyapatite growing, porous structure with smooth surface of silk fibroin scaffolds was noticed as illustrated in Figure 5.15(a)-(b). The pore size of scaffold structure represented the size of salt crystals used (600-710μm). The outer surface of salt-leached silk fibroin scaffolds before hydroxyapatite growing, shown in Figure 5.15(c), was similar to the inner surface of scaffolds as presented in Figure 5.15(a). After alternate soaking in calcium and phosphate solutions, the pore size of scaffolds decreased as seen from both inner surface (Figure 5.15(d), (g), and (j)) and outer surface (Figure 5.15(f), (i), and (l)). This due to the infusion of calcium and phosphate solutions throughout the scaffolds leading to the deposition of hydroxyapatite on the surface of scaffolds. The accumulated hydroxyapatite resulted in the rough surface of porous structure as seen in Figure 5.15(e), (h), and (k). After 6 cycles of alternate soaking, the outer structure of scaffolds was covered with hydroxyapatite. As a result, the alternate soaking process

could not be further performed; i.e. calcium and phosphate solutions hardly diffused into the scaffolds.

Considering the hydroxyapatite crystals grown on the scaffold surface after 2, 4, and 6 cycles of alternate soaking (Figure 5.16), it was found that the hydroxyapatite formed inside the scaffolds looked to be less than that grown on the outer surface. Size of hydroxyapatite crystal seemed to increase as increasing the number of alternate soaking cycles from 2 to 4 cycles as shown in Figure 5.16(b), and (d). After 6 cycles of alternate soaking (Figure 5.16(f)), the more accumulation of hydroxyapatite crystals led to a thick layer of hydroxyapatite fully filled the porous structure as discussed earlier.

5.5.1.2 Hydroxyapatite-conjugated gelatin/silk fibroin scaffolds

Figure 5.17 showed the cross sectional morphology of hydroxyapatite-conjugated gelatin/silk fibroin scaffolds. The structure of CGSF0 was very fibrous (Figure 5.17(a)-(b)). Conjugated gelatin was partly formed fibers inside the pores of silk fibroin scaffolds resulting in fiber-like structure with highly interconnection which was different from the porous structure of silk fibroin as shown in Figure 5.15(a)-(b). Figure 5.17(c) showed the outer surface of CGSF0 which obviously differed from the inner surface of CGSF0 in Figure 5.17(a) and the outer surface of SF0 in Figure 5.15(c). Gelatin conjugating caused a less opened-surface of scaffolds. This partly limited the infusion of calcium and phosphate solution into the scaffolds. After hydroxyapatite growing, the interconnected porous network tended to decrease comparing to CGSF0 (Figure 5.17(d), (g), and (j)). The deposition of hydroxyapatite was observed along gelatin fiber and scaffold surface leading to a rough surface (Figure 5.17(e), (h), and (k)). More hydroxyapatite accumulation was noticed upon the increasing number of alternate soaking cycles. The accumulation of hydroxyapatite over the outer surface of scaffolds was clearly noticed which caused the porous structure disappeared as presented in Figure 5.17(f), (i), and (l). This result revealed that gelatin conjugating on silk fibroin scaffolds influenced the morphology of silk fibroin scaffolds and the pattern of hydroxyapaptite growing.

Figure 5.18 elucidated the hydroxyapatite crystals grown on the conjugated gelatin/silk fibroin scaffold surface after 2, 4, and 6 cycles of alternate soaking. It confirmed that the hydroxyapatite deposition inside the scaffolds was less than that formed on the outer surface of the scaffolds. The hydroxyapatite crystal aggregation increased as increasing the number of alternate soaking cycles as shown in Figure 5.18(b), (d), and (f).

Comparing the hydroxyapatite crystals grown in SF (Figure 5.16) and CGSF (Figure 5.18), it was noted that crystal sizes of hydroxyapatite in SF were larger than those in CGSF. This could be a result from a difference in the morphology of both scaffolds. Moreover, the surface area of fibrous CGSF was relatively more than that of SF, while the pore volume of CGSF was less as noticed from an increased weight of scaffolds (~13%) after gelatin conjugating. This ensured that gelatin conjugating of silk fibroin scaffolds influenced hydroxyapatite growing including the size and distribution of hydroxyapatite.

Additionally, after the silk fibroin and conjugated gelatin/silk fibroin scaffolds were immersed in calcium and phosphate solutions, i.e. hydroxyapatite growing, the average weight of the scaffolds was increased as depicted in Figure 5.19. The increasing weight of silk fibroin and conjugated silk fibroin scaffolds after various numbers of alternate soaking cycles was obviously the weight of grown hydroxyapatite in the scaffolds. It was clearly seen that the weight of hydroxyapatite deposited in the scaffolds was progressively increased upon the increasing number of alternate soaking cycles.

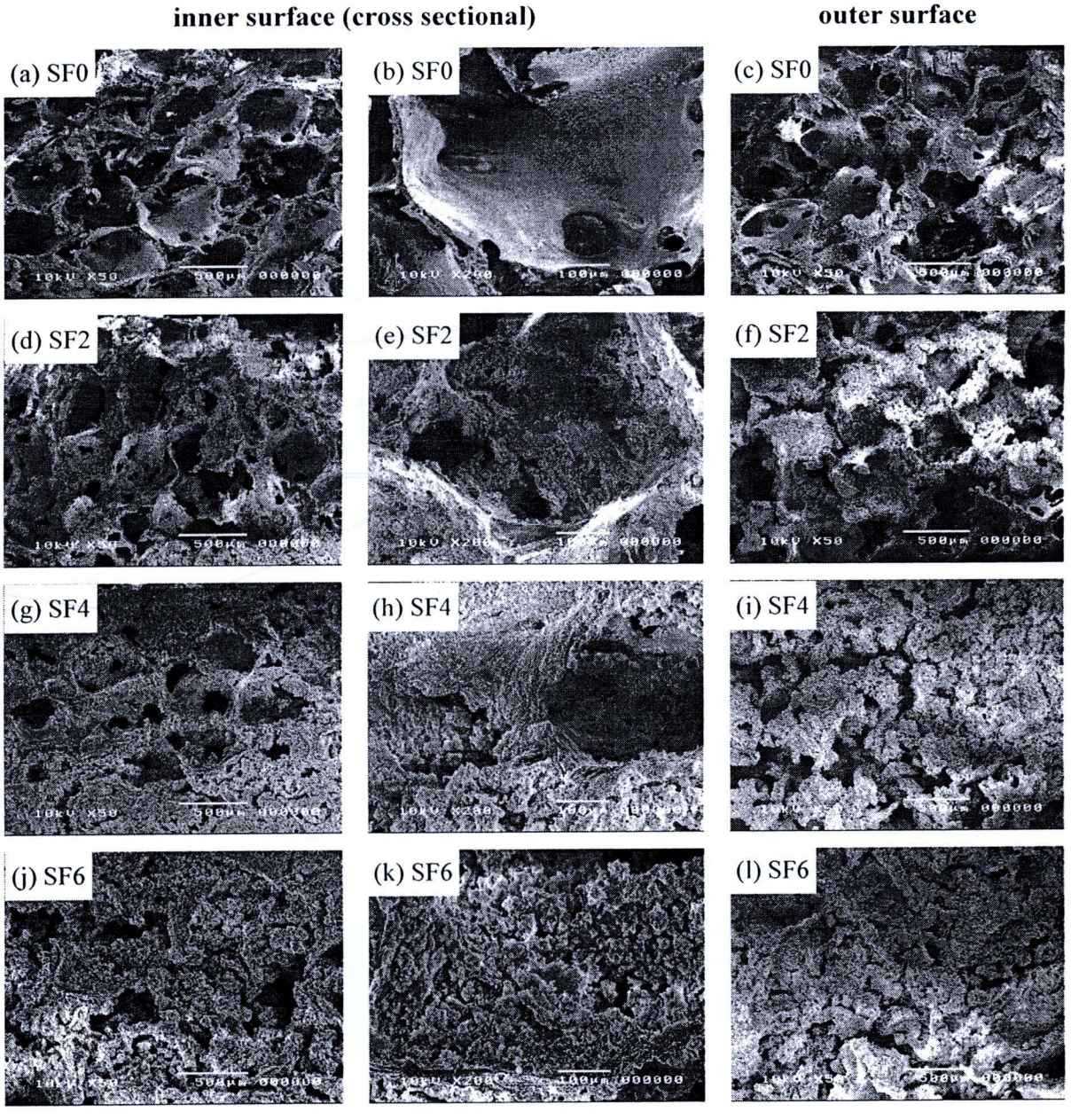

Figure 5.15 SEM micrographs of silk fibroin scaffolds (a)-(c) before soaking, after (d)-(f) 2 cycles, (g)-(i) 4 cycles, and (j)-(l) 6 cycles of alternate soaking in calcium and phosphate solutions.

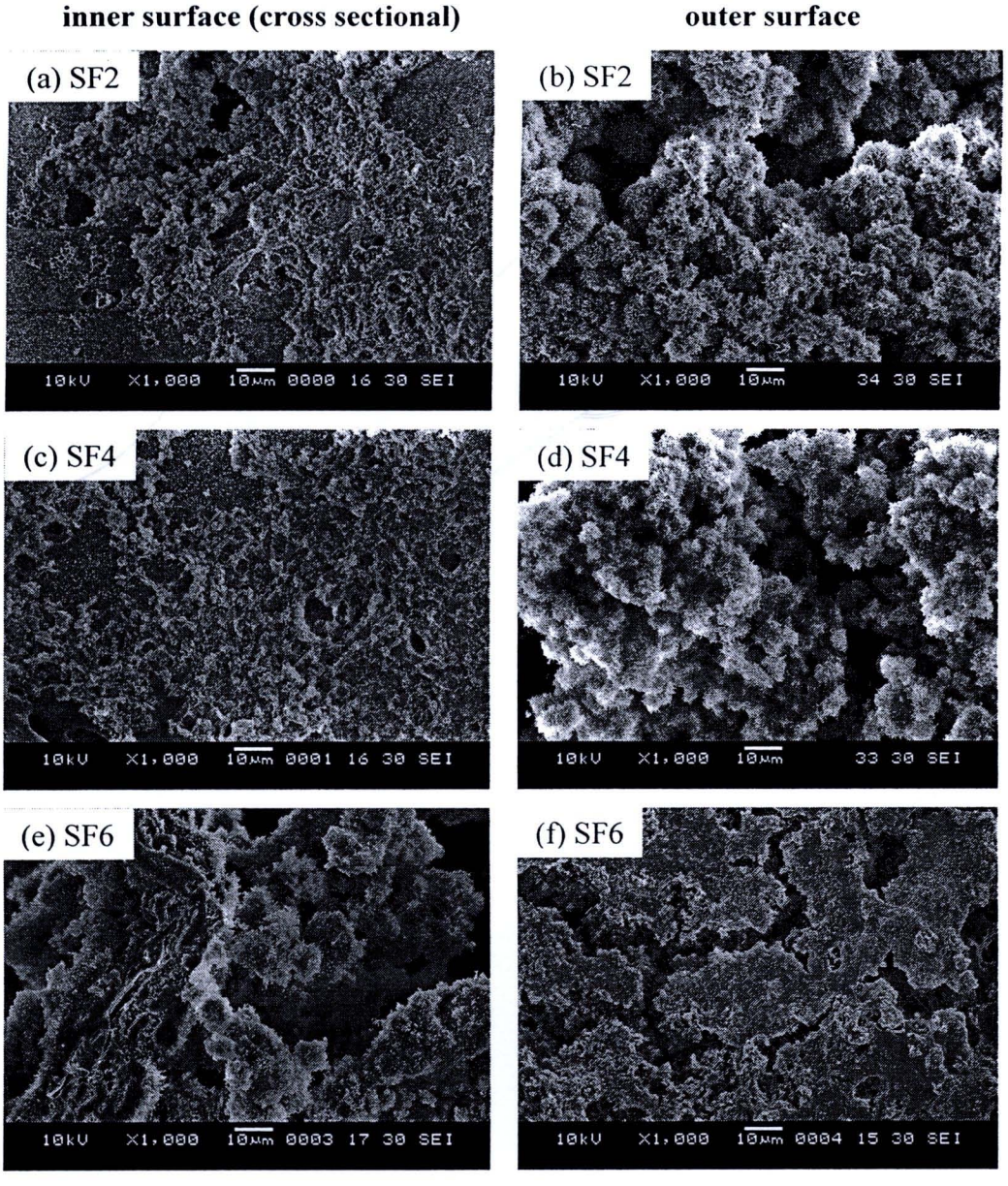

Figure 5.16 SEM micrographs of hydroxyapatite crystals in silk fibroin scaffolds (a)-(b) 2 cycles, (c)-(d) 4 cycles, and (e)-(f) 6 cycles of alternate soaking.

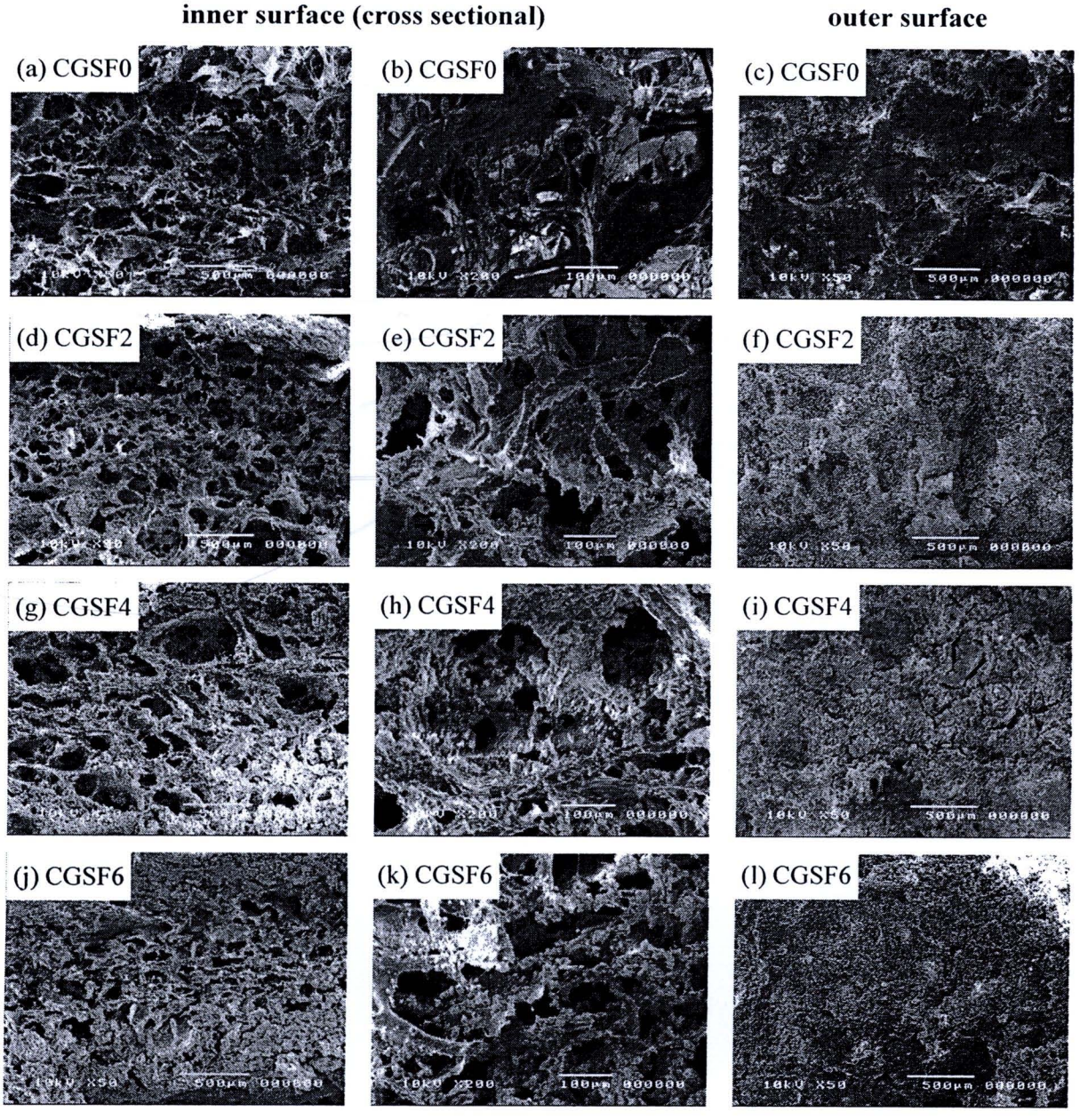

Figure 5.17 SEM micrographs of conjugated gelatin/silk fibroin scaffolds (a)-(c) before soaking, after (d)-(f) 2 cycles, (g)-(i) 4 cycles, and (j)-(l) 6 cycles of alternate soaking in calcium and phosphate solutions.

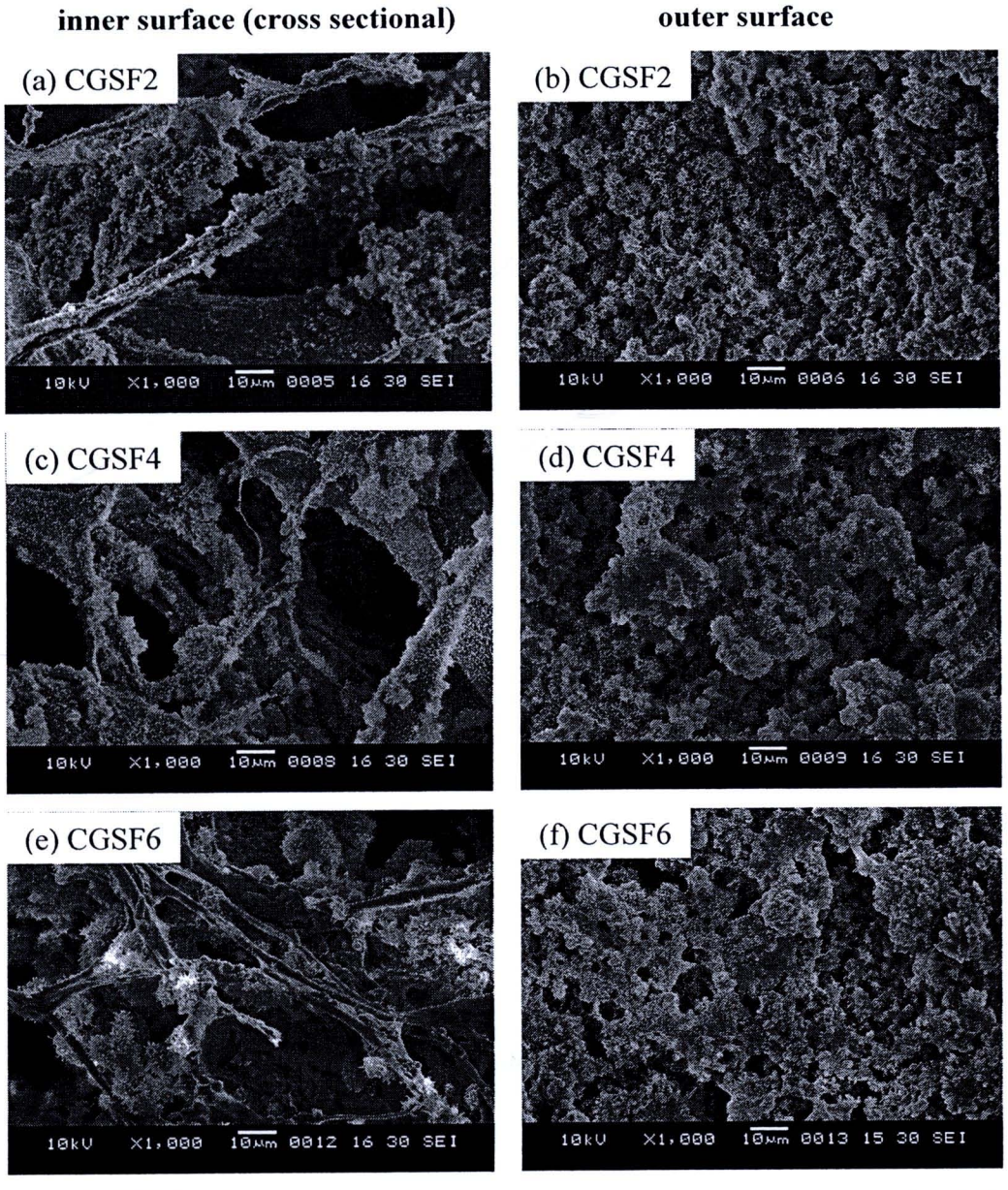

Figure 5.18 SEM micrographs of hydroxyapatite crystals in conjugated gelatin/silk fibroin scaffolds (a)-(b) 2 cycles, (c)-(d) 4 cycles, and (e)-(f) 6 cycles of alternate soaking.

The comparison between SF and CGSF exhibited that the increasing weight of hydroxyapatite in SF was higher than CGSF and the difference tended to be more as increasing the cycles of alternate soaking process. The weight of both scaffolds was increased about 80-95% after 2 cycles of alternate soaking. At 6 cycles of alternate soaking, hydroxyapatite deposited in SF and CGSF scaffolds were 230% and 190% of initial weight of scaffolds, respectively. When SF was conjugated with gelatin, the ability of hydroxyapatite growing via solution infusion into the scaffolds was reduced. This was in agreement with the results on SEM micrographs of both types of scaffolds discussed previously.

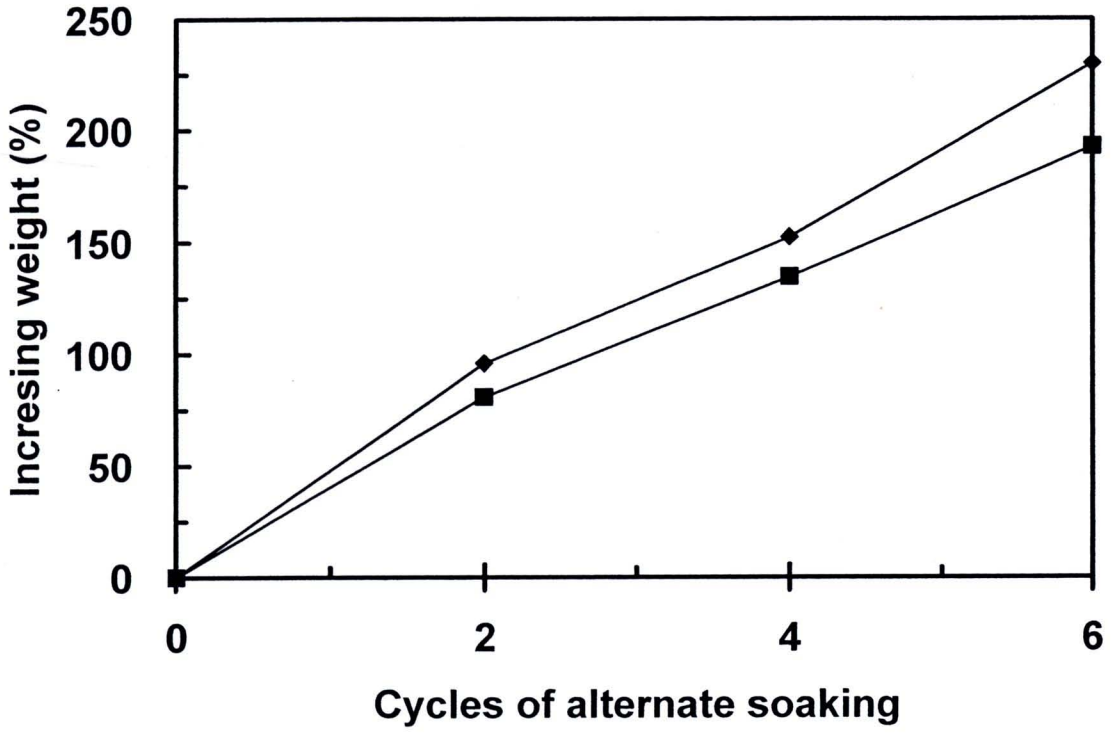

Figure 5.19 Increasing weights of scaffolds as a function of alternate soaking cycles (♦) silk fibroin scaffolds, and (■) conjugated gelatin/silk fibroin scaffolds.

Our results corresponded to a recent report by Furuzono *et.al.* [57] which showed the increasing of apatite weight on the silk fabric with alternated soaking repetitions. Taguchi *et.al.* [11] also reported that hydroxyapatite content increased with increasing immersion cycle in calcium and phosphate solutions.

5.5.2 Compressive modulus of scaffolds

The compressive modulus of hydroxyapatite/silk fibroin and hydroxyapatite-conjugated gelatin/silk fibroin scaffolds was shown in Figure 5.20. The compressive modulus of SF0 and CGSF0 were 262.50±61.85 and 506.00±151.10 kPa, respectively. This could be a result from the morphology of both scaffolds. Morphology of CGSF was more fibrous structure and the surface area of CGSF was more than SF. This supported compressive ability of scaffolds. Moreover, CGSF was treated by DHT and EDC. DHT brings about chemical bonding between the amino and carboxyl groups within molecule of polypeptide. It was well-known that crosslinking could enhance mechanical properties of scaffolds. Further treated with EDC, the primary amines on the peptides formed a stable amide bond between the peptide of gelatin and silk fibroin [47] causing an increasing in compressive modulus of scaffolds.

Comparing the compressive modulus of salt-leached silk fibroin scaffolds to the other work reported [1], it was found that the compressive modulus of SF0 was lower than that reported (770±50 kPa). This might due to different testing condition and the size of scaffolds. Our scaffolds were rather small (~11mm in diameter, ~2mm in height) comparing to those used in Kim *et.al.*'s work (12mm in diameter, 10mm in height). Another possible reason might be the different source of *Bombyx mori* silkworm. Our Thai silkworm (yellow cocoon) possessed lower molecular weight (~253.4 kDa) than that of Japanese race (white cocoon, ~515.1 kDa) [65].

After hydroxyapatite growing, compressive modulus of both scaffolds increased with an increasing numbers of alternate soaking cycles. At 6 cycles of alternate soaking, compressive modulus of SF increased by 100% while that of CGSF increased 60%. This

might be the influence of the hydroxyapatite deposited in SF which was more than in CGSF. However, the absolute compressive modulus of SF6 (535.00±93.99 kPa) was still lower than that of CGSF6 (826.00±388.63 kPa). These results confirmed that gelatin conjugating and hydroxyapatite growing on silk fibroin scaffolds enhanced the compressive modulus of silk fibroin scaffolds.

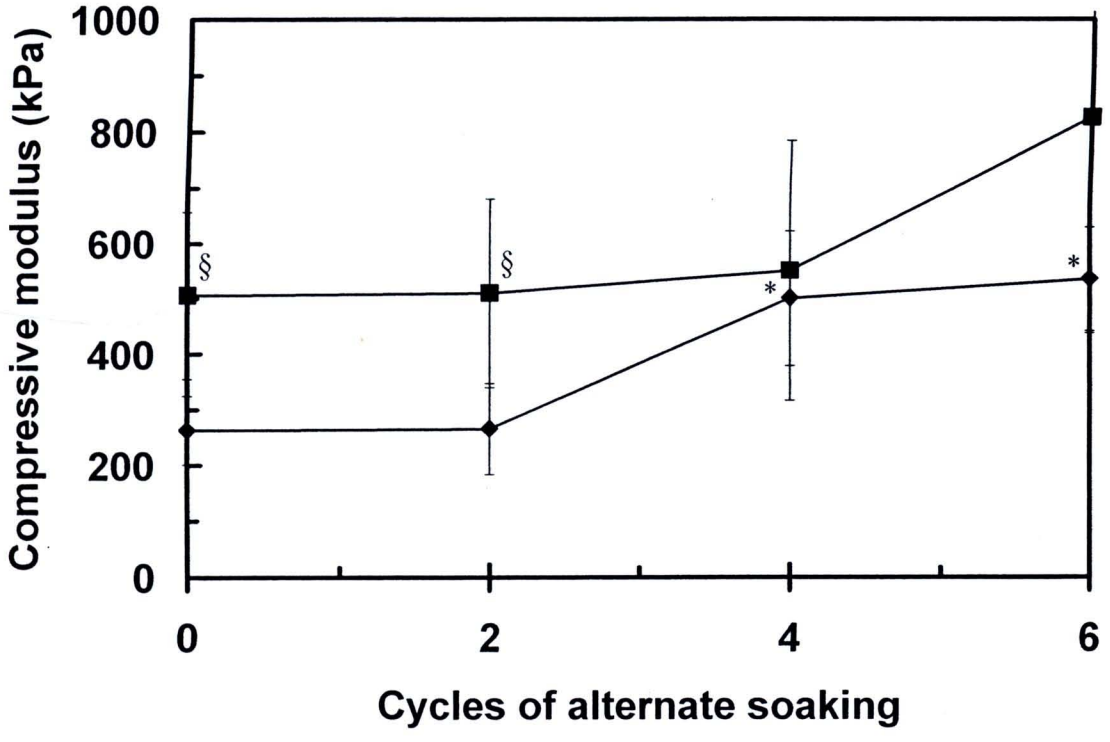

Figure 5.20 Compressive modulus of (♦) hydroxyapatite/silk fibroin scaffolds, and (■) hydroxyapatite-conjugated gelatin/silk fibroin scaffolds.

* represent the significant difference ($p<0.05$) relative to each scaffold before alternate soaking (0 cycle).

§ represent the significant difference ($p<0.05$) relative to the scaffold at the same number of alternate soaking cycles

5.5.3 Swelling property of scaffolds

Figure 5.21 showed the swelling ratio of hydroxyapatite/silk fibroin scaffolds and hydroxyapatite-conjugated gelatin/silk fibroin scaffolds at various numbers of alternate soaking cycles. The swelling ratios of SF0 and CGSF0 were 11.02±1.46 and 10.32±1.37, respectively. The swelling ratio of SF was very similar to that of CGSF0. This result showed that gelatin conjugating did not affect the swelling property of scaffolds.

After hydroxyapatite growing, swelling ratio of both SF and CGSF decreased significantly with an increasing numbers of alternate soaking cycles. At 6 cycles of alternate soaking, swelling ratio of SF and CGSF decreased about 50-60%. It was a result from the accumulation of hydroxyapatite on the surface of scaffolds obstructed the swelling ability of scaffolds and possibly the less pore volume in the scaffolds as seen from SEM micrographs.

Comparing the swelling property of salt-leached silk fibroin scaffolds to the other work reported [1], it was found that the swelling ratio of SF0 was lower than that prepared from Japanese white silkworm (28.4±2.7). The discrepancy might be attributed by different source of silk fibroin as well as the testing condition. Before the swelling test, our scaffolds were not dried in a vacuum oven to reduce the humidity. This could reduce the swelling ability of our silk fibroin scaffolds. In addition, our scaffolds were rather small (~11mm in diameter, ~2mm in height) comparing to those used in Kim *et.al.*'s work (12mm in diameter, 10mm in height).

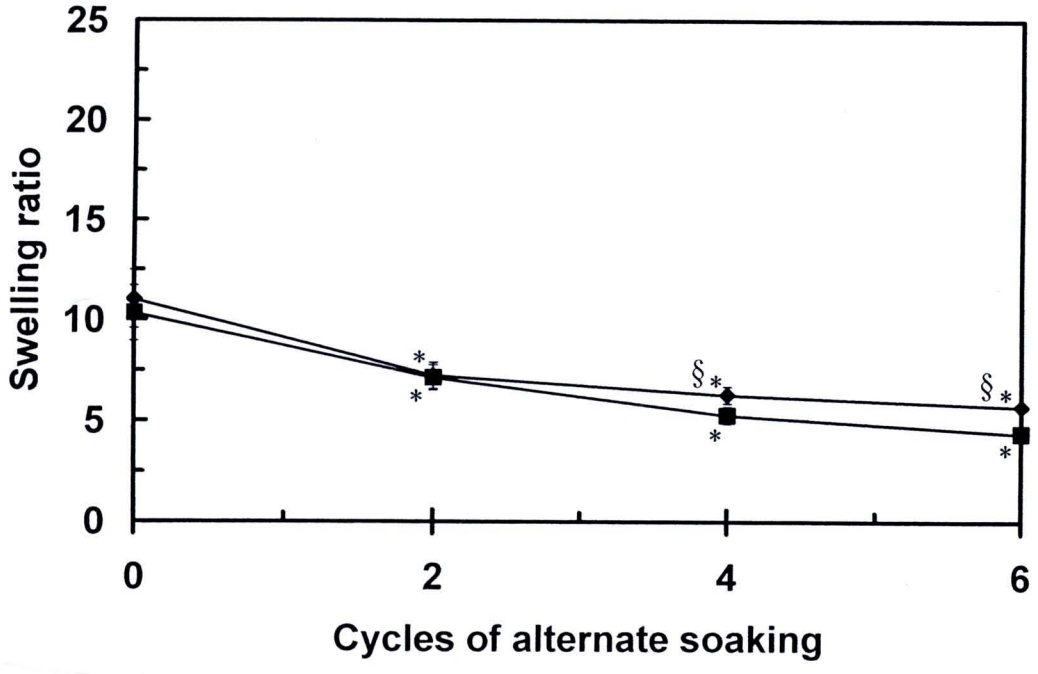

Figure 5.21 Swelling properties of (♦) hydroxyapatite/silk fibroin scaffolds, and (■) hydroxyapatite-conjugated gelatin/silk fibroin scaffolds.

* represent the significant difference ($p<0.05$) relative to each scaffold before alternate soaking (0 cycle).

§ represent the significant difference ($p<0.05$) relative to the scaffold at the same number of alternate soaking cycles

5.5.4 Biological property of scaffolds

5.5.4.1 MC3T3-E1 proliferation tests

Figure 5.22 presented the numbers of MC3T3-E1 on hydroxyapatite/silk fibroin scaffolds, and hydroxyapatite-conjugated gelatin/silk fibroin scaffolds after 1, 7 and 14 days of the culture. At 1 day after seeding, no significant difference in the number of cells among various scaffolds was noticed except CGSF4. At 7, and 14 days after seeding, the number of cells tended to decrease in all scaffolds except in CGSF0. This might be the

result of fibrous morphology of CGSF0 which was reported to support the proliferation of MC3T3-E1 [66]. In addition, hydrophilic property of gelatin promoted cell proliferation of CGSF0. Calvert *et.al.* [67] reported that MC3T3-E1 could adhere better on hydrophilic surfaces than hydrophobic surfaces. Moreover, gelatin contains arginine-glycine-aspartic acid (RGD)-like sequence that promotes cell adhesion and migration [46, 68]. For the case of hydroxyapatite/silk fibroin and hydroxyapatie-conjugated gelatin/silk fibroin scaffolds, cells might not be able to proliferate on scaffolds due to a high deposition of hydroxyapatite on the cell-seeding surface of scaffolds.

The other work reported on the use of Thai silk fibroin in tissue engineering by Meechaisue *et.al.* [53] have showed that MC3T3-E1 could adhere and proliferate on the electrospun Nang-Lai silk fibroin fiber mats similar to that on electrospun silk fibroin fiber mats from Chinese/Japanese hybrid silkworms. They suggested that the electrospun Nang-Lai silk fibroin fiber mats could be used as scaffolding materials for bone cell culture.

5.5.4.2 MC3T3-E1 migration and morphological observation

Figure 5.23-5.25 showed SEM micrographs of spreading behavior of MC3T3-E1 mouse osteoblast-like on silk fibroin scaffolds, and conjugated gelatin/silk fibroin scaffolds after 14 days of culture. Conjugated gelatin/silk fibroin scaffolds which showed the highest cell proliferation were selected to observe the cell interaction and morphology. Furthermore, silk fibroin scaffolds, as control, were investigated. For silk fibroin scaffold as shown in Figure 5.23, MC3T3-E1 was found throughout the thickness of scaffolds (position 1 to 4) though there were fewer cells found at the deepest position (position 4). For the case of conjugated gelatin/silk fibroin scaffolds, the surfaces were decorated with cells. In addition, the porous structure in the upper half of conjugated gelatin/silk fibroin scaffolds (Figure 5.24(a)-(b)) was disappeared as it was possibly covered with neo-extracellular matrix deposited by MC3T3-E1. Comparing the cell morphology proliferated on both types of scaffolds shown in Figure 5.25, it was evident

that cells on silk fibroin surface were round. No filopodia was observed as shown in Figure 5.25(a). Meanwhile, the extension of cytoplasm on conjugated gelatin/silk fibroin surfaces was noticed as seen in Figure 5.25(b). Cell morphology implied that cells were more active on conjugated gelatin/silk fibroin surfaces. For the case of hydroxyapatite/silk fibroin and hydroxyapatie-conjugated gelatin/silk fibroin scaffolds, no cells inside scaffolds were noticed. This confirmed that the hydroxyapatite accumulation on the outer surface of scaffolds obstructed the cell migration into the scaffolds. This possibly ceased the cell growth resulting in a decreasing trend in the number of living cells as noticed in previous section (Figure 5.22)

This result indicated that gelatin conjugating on silk fibroin scaffolds promoted the proliferation and biological activity of mouse osteoblast-like cells. Further investigations are required to fully understand the biological activity of cells on these scaffolds.

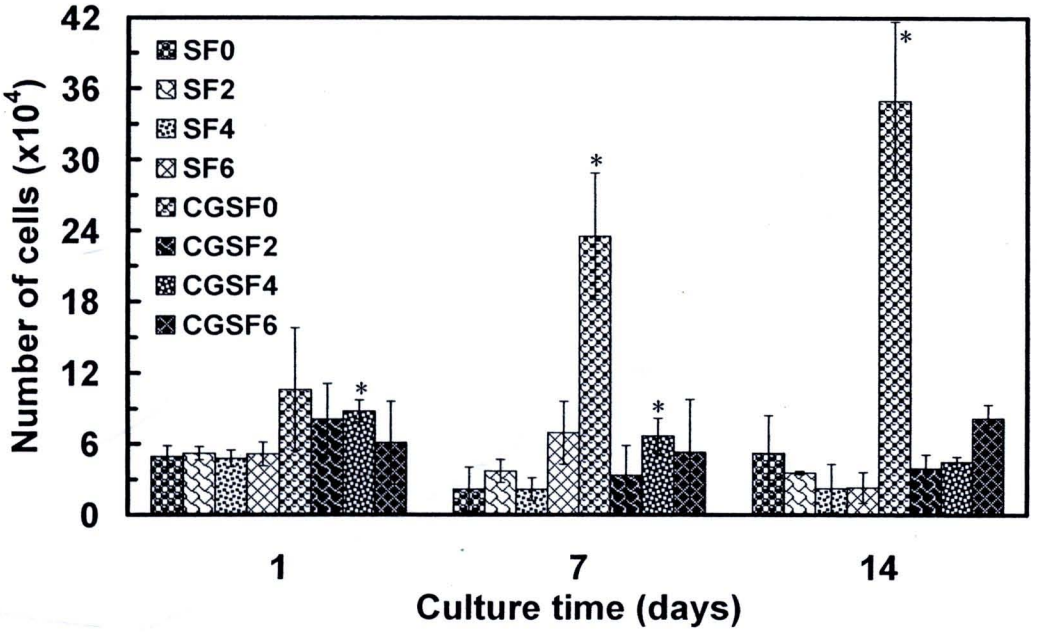

Figure 5.22 Number of MC3T3-E1 on hydroxyapatite/silk fibroin scaffolds, and hydroxyapatite-conjugated gelatin/silk fibroin scaffolds after 1, 7, and 14 days of the culture (seeding: 2×10^4 cells/scaffold).

* represent the significant difference ($p<0.05$) relative to silk fibroin (SF0) scaffolds in each periods.

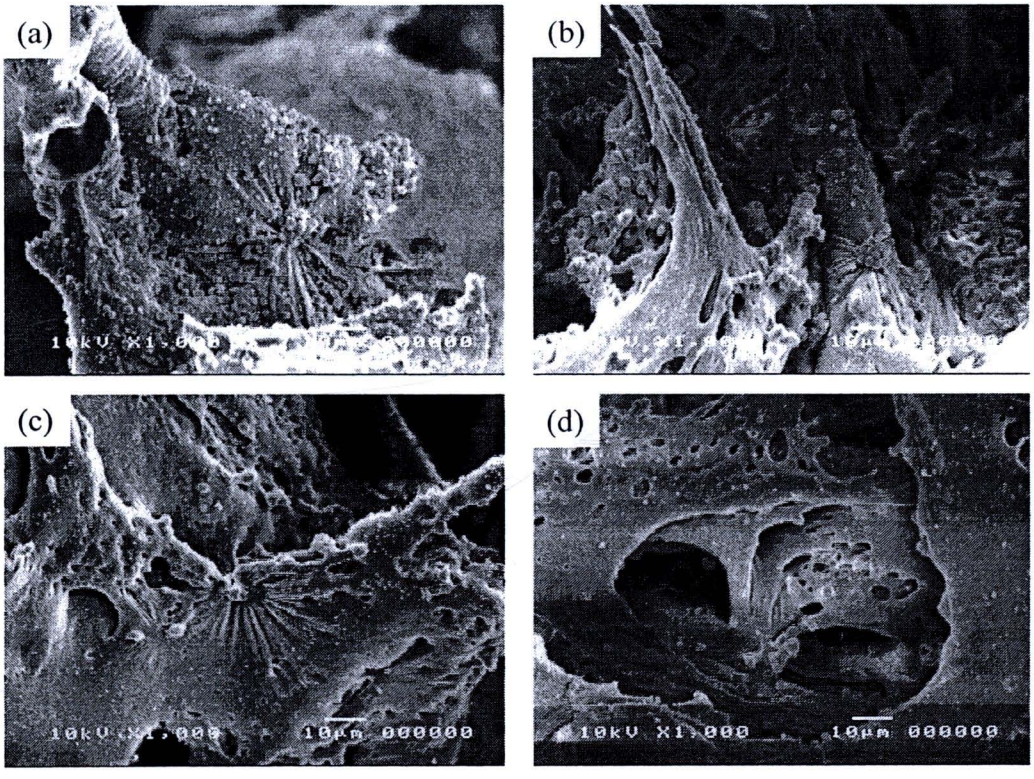

Figure 5.23 SEM micrographs of cross-sectional plane of silk fibroin scaffolds at position (a) 1 (cell seeding side), (b) 2, (c) 3, and (d) 4 (plate-exposed side) after 14 days of MC3T3-E1 culture.

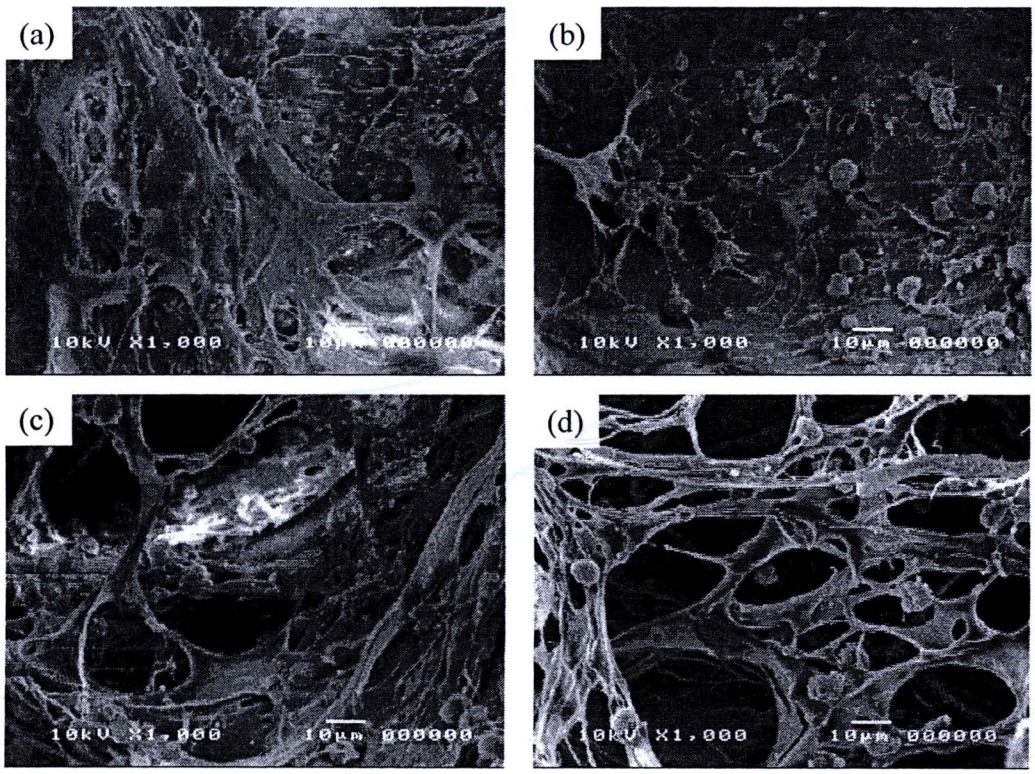

Figure 5.24 SEM micrographs of cross-sectional plane of conjugated-gelatin silk fibroin scaffolds at position (a) 1 (cell seeding side), (b) 2, (c) 3, and (d) 4 (plate-exposed side) after 14 days of MC3T3-E1 culture.

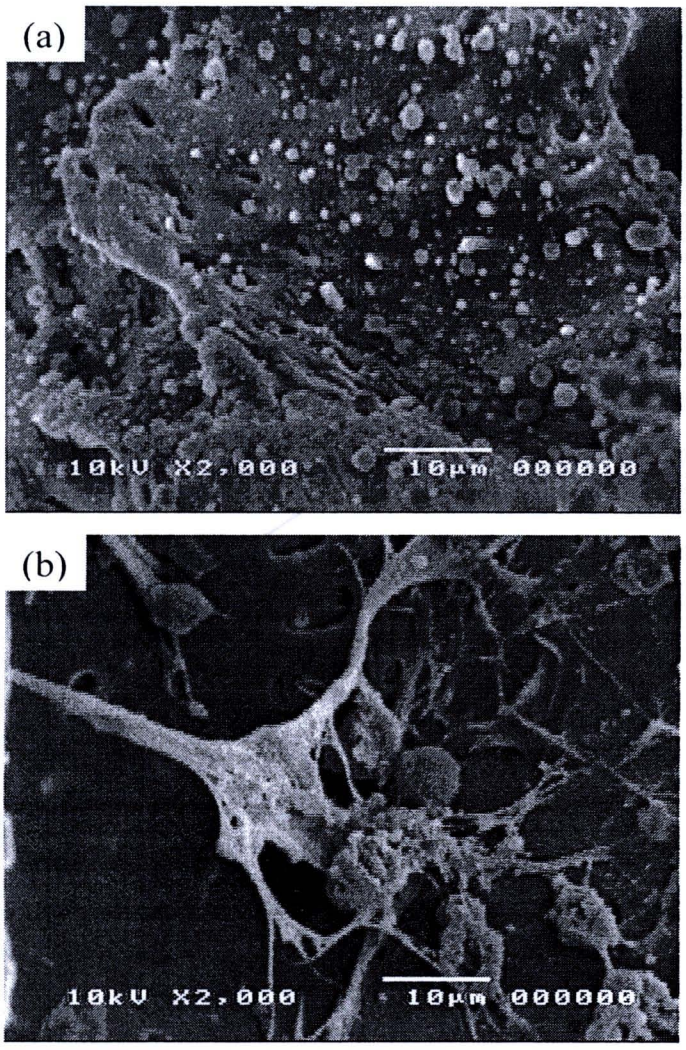

Figure 5.25 SEM micrographs of MC3T3-E1 morphology after 14 days cultured on scaffolds: (a) silk fibroin, and (b) conjugated-gelatin silk fibroin scaffolds.